The CDK inhibitor CR8 mediates cyclin K degradation through the CUL4-RBX1-DDB1 E3 ubiquitin ligase

Mikołaj Słabicki†[1-3], Zuzanna Kozicka†[4,5], Georg Petzold†[4], Yen-Der Li[1,2,6], Manisha Manojkumar[1-3], Richard Bunker[4,7], Katherine A. Donovan[8,9], Quinlan L. Sievers[1,2], Jonas Koeppel[1-3], Dakota Suchyta[4,5], Adam S. Sperling[1,2], Jessica A. Gasser[1,2], Li R. Wang[1], Steven M. Corsello[1,2], Rob S. Sellar[1,2,10], Max Jan[1,2], Emma C. Fink[1,2], Dennis Gillingham[5], Claudia Scholl[11], Stefan Fröhling[3,12], Todd R. Golub[1,13,14], Eric S. Fischer[8,9], Nicolas H. Thomä*[4], Benjamin L. Ebert*[1,2,14]

† These authors contributed equally to this work.

*Corresponding author. Email: benjamin_ebert@dfci.harvard.edu (B.L.E.); nicolas.thoma@fmi.ch (N.H.T.)

Affiliations:

[1]Broad Institute of MIT and Harvard, Cambridge, MA;

[2]Department of Medical Oncology, Dana-Farber Cancer Institute, Boston, MA;

[3]Division of Translational Medical Oncology, German Cancer Research Center (DKFZ) and National Center for Tumor Diseases (NCT), 69120 Heidelberg, Germany;

[4]Friedrich Miescher Institute for Biomedical Research, Basel, Switzerland;

[5]University of Basel, Basel, Switzerland;

[6]Department of Molecular and Cellular Biology, Harvard University, Cambridge, MA;

[7]Current address: Monte Rosa Therapeutics, Basel, Switzerland;

[8]Department of Biological Chemistry and Molecular Pharmacology, Harvard Medical School, Boston, MA;

[9]Department of Cancer Biology, Dana-Farber Cancer Institute, Boston, MA 02215, USA;

[10]Department of Hematology, UCL Cancer Institute, University College London, London WC1E 6DD, UK;

[11]Division of Applied Functional Genomics, German Cancer Research Center (DKFZ) and National Center for Tumor Diseases (NCT), 69120 Heidelberg, Germany;

[12]German Cancer Consortium, 69120 Heidelberg, Germany;

[13]Department of Pediatric Oncology, Dana-Farber Cancer Institute, Boston, MA;

[14]Howard Hughes Medical Institute, Boston, MA.

35   **Abstract**

36   Molecular glue compounds induce protein-protein interactions that, in the context of a

37   ubiquitin ligase, lead to protein degradation. Unlike traditional enzyme inhibitors, such

38   molecular glue degraders act sub-stoichiometrically to catalyse rapid depletion of previously

39   inaccessible targets. They are clinically effective and highly sought-after, but have thus far only

40   been discovered serendipitously. Through systematic mining of databases for correlations

41   between the cytotoxicity of 4,518 compounds and E3 ligase expression levels across hundreds

42   of human cancer cell lines, we identified CR8, a cyclin-dependent kinase (CDK) inhibitor, as

43   a compound that acts as a molecular glue degrader. A solvent-exposed pyridyl moiety of CR8,

44   in its CDK-bound form, induces CDK12-cyclin K complex formation with DDB1, the CUL4

45   adaptor protein, bypassing the requirement for a substrate receptor and presenting cyclin K

46   (cycK) for ubiquitination and degradation. Our studies demonstrate that chemical alteration of

47   surface-exposed moieties can confer gain-of-function glue properties to an inhibitor, and we

48   propose this as a broader strategy to turn target binders into molecular glues.

49

50

51

52

Molecular glues are a class of small molecule drugs that induce or stabilise protein-protein interactions[1]. In the context of a ubiquitin ligase, drug-induced interactions can lead to protein degradation, which is an emerging strategy for the inactivation of therapeutic targets intractable by conventional pharmacological means[2,3]. Known molecular glue degraders bind to substrate receptors of E3 ubiquitin ligases and recruit target proteins for their ubiquitination and subsequent degradation by the proteasome.

Thalidomide analogues and aryl sulphonamides are two classes of drugs that act as molecular glue degraders. Widely used in the clinic, thalidomide analogues have proven to be an effective treatment for multiple myeloma, other B cell malignancies, and myelodysplastic syndrome with a deletion in chromosome 5q[4]. Thalidomide analogues recruit zinc-finger transcription factors and other targets to CRBN[5–8], the substrate receptor of the cullin-RING E3 ubiquitin ligase CUL4A/B-RBX1-DDB1-CRBN (CRL4^{CRBN})[9]. Similarly, aryl sulphonamides degrade the essential RNA-binding protein RBM39 by engaging DCAF15, the substrate receptor of the CRL4^{DCAF15} E3 ubiquitin ligase[10–12]. In these examples, the degraders are not dependent on a ligandable pocket on the target protein, but instead leverage complementary protein-protein interfaces between the receptor and the target. By reprogramming ubiquitin ligase selectivity, these molecules divert the ligase to drive multiple rounds of target ubiquitination in a catalytic manner[13]. Such compounds can thus circumvent limitations of classical inhibitors, expanding the repertoire of "druggable" proteins. Although highly sought-after, molecular glue degraders have only been found serendipitously, and there are currently limited strategies available for identifying or designing such compounds.

CR8 induces proteasomal cycK degradation

To identify small molecules that mediate targeted protein degradation through an E3 ubiquitin ligase, we correlated drug sensitivity data for 4,518 clinical and pre-clinical drugs tested against 578 cancer cell lines[14,15] with the mRNA expression levels for 499 E3 ligase components[16] (**Extended Data Fig. 1a**). *DCAF15* gene expression correlated with indisulam and tasisulam toxicity, consistent with its known function as a degrader of the essential protein RBM39 by the CRL4^{DCAF15} E3 ubiquitin ligase, thus demonstrating the potential of the approach (**Extended Data Fig. 1b, c).** We sought to validate the high-scoring ligase-drug correlations by examining whether CRISPR-mediated inactivation of the identified E3 ligase component would rescue the respective drug-induced toxicity (**Extended Data Fig. 1d**). These experiments confirmed that sgRNAs targeting *DCAF15* confer resistance to indisulam and tasisulam. In addition, we also observed a correlation between cytotoxicity of the CDK-inhibitor *R*-CR8 and mRNA expression levels of the CUL4 adaptor DDB1 (**Fig. 1a and Extended Data Fig. 1e**). Consistently, sgRNAs targeting *DDB1* conferred resistance to *R*-CR8[17] (**Fig. 1b**).

As DDB1-dependent cytotoxicity of *R*-CR8 implicated ubiquitin ligase-mediated degradation of one or more essential proteins, we performed quantitative proteome-wide mass spectrometry to evaluate protein abundance following compound treatment. Of the >8,000 quantified proteins, cycK was the only protein that consistently showed decreased abundance following *R*-CR8 addition (**Fig. 1c and Extended Data Fig. 1f, g**). As expected, *R*-CR8 did not alter the cycK mRNA levels (**Extended Data Fig. 1h)** and compound-induced cycK degradation could be rescued by inhibition of the E1 ubiquitin-activating enzyme (MLN7243), cullin neddylation (MLN4924) and the proteasome (MG132) (**Fig. 1d**). Together, these results suggest that *R*-CR8 triggers rapid proteasomal degradation of cycK (**Fig. 1e**) through the activity of a DDB1-containing cullin-RING ubiquitin ligase.

To dissect the molecular machinery required for *R*-CR8 toxicity, we performed genome-wide and E3 ubiquitin ligase-focused CRISPR-Cas9 resistance screens (**Fig. 1f and Extended Data Fig. 2a, b**). SgRNAs targeting *DDB1*, *CUL4B*, *RBX1*, the cullin-RING activator *NEDD8*, and the NEDD8-activating enzyme (*NAE1/UBA3*) were significantly enriched in the *R*-CR8-resistant cell population. These proteins are all required for CRL activity, and our results thus provide genetic evidence for the involvement of a functional CUL4-RBX1-DDB1 ubiquitin ligase complex in mediating *R*-CR8 cytotoxicity.

Thus far, all known cullin-RING ligases engage their substrates through specific substrate receptors, and DDB1 serves as an adaptor protein able to bind over 20 different

109   substrate receptors (also known as DDB1-CUL4-associated-factors, DCAFs)[17,18] to recruit
110   them to the CUL4-RBX1 E3 ubiquitin ligase core. As no DCAF was identified in our viability
111   screens, we constructed a fluorescent reporter of cycK stability (**Extended Data Fig. 2c**), in
112   which *R*-CR8-mediated degradation of endogenous cycK could be recapitulated with a
113   cycK$_{eGFP}$ fusion protein (**Fig. 1d, e and Extended Data Fig. 2d-f**). Using the stability reporter,
114   in which the extent of degradation can be determined by measuring cycK$_{eGFP}$ levels normalised
115   to mCherry expression, we found that *S*- and *R*-CR8 facilitated cycK$_{eGFP}$ degradation to the
116   same extent (**Extended Data Fig. 2g**; henceforth, CR8 refers to *R*-CR8). We then performed
117   a genome-wide CRISPR-Cas9 screen for genes involved in cycK reporter stability and
118   validated the involvement of DDB1 in CR8-mediated cycK degradation (**Fig. 1g, Extended**
119   **Data Fig. 2h),** but not in compound-independent cycK degradation (**Extended Data Fig. 2i**).
120   In addition, we identified cyclin-dependent kinase 12 (CDK12), which is a known target of
121   CR8[19] and whose activity depends on the interaction with cycK, as a crucial component for
122   CR8-induced cycK$_{eGFP}$ destabilisation (**Fig. 1g, Extended Data Fig. 2h-k**).
123   As neither the cycK$_{eGFP}$ stability reporter screen nor the CR8 resistance screen
124   identified a substrate receptor, we performed additional CRISPR screens targeting 29 genes
125   encoding known DCAFs or DCAF-like candidate proteins in four different cell lines. While
126   sgRNAs targeting the previously identified components of the CUL4-RBX1-DDB1 complex
127   consistently caused resistance to CR8, a DCAF substrate receptor could not be identified
128   (**Extended Data Fig. 3**).
129

CR8 directs CDK12 to CRL4 core component

131   Since none of our genetic screens highlighted a DCAF required for cycK degradation, we tested
132   whether CR8-engaged CDK12-cycK directly binds one of the CUL4-RBX1-DDB1 ligase
133   components in the absence of a substrate receptor. We therefore performed *in vitro* co-
134   immunoprecipitation experiments using recombinantly purified proteins. The kinase domain
135   of CDK12 (CDK12$^{713-1052}$) bound to cycK$^{1-267}$ did not markedly enrich DDB1 over the bead
136   binding control in the absence of CR8, whereas equimolar amounts of the compound led to
137   stoichiometric complex formation (**Fig. 2a**). DDB1 β-propeller domains A (BPA) and C
138   (BPC)[20], which are otherwise involved in DCAF binding, were sufficient for drug-induced
139   CDK12-cycK recruitment. DDB1 β-propeller B (BPB), which binds CUL4 and is not involved
140   in DCAF binding, was dispensable for the drug-dependent interaction with CDK12-cycK (**Fig.**
141   **2a**). *In vitro* ubiquitination assays confirmed that the CUL4A-RBX1-DDB1 ligase core alone

142 is sufficient to drive robust cycK ubiquitination (**Fig. 2b**). Quantification of the interaction
143 showed that CR8 stimulated binding between CDK12-cycK and DDB1 in the range of 100-
144 500 nM depending on the experimental setup (**Fig. 2c and Extended Data Fig. 4**). While weak
145 CDK12-cycK-DDB1 interaction was still detectable in the absence of the compound *in vitro*,
146 CR8 strengthened complex formation 500- to 1000-fold as estimated by isothermal titration
147 calorimetry (ITC) (**Extended Data Fig. 4f**). Thus, our data indicate that CR8-engaged CDK12-
148 cycK is recruited to the CUL4-RBX1-DDB1 ligase core through DDB1, and the compound
149 tightens the complex sufficiently to drive CR8-induced cycK degradation in the absence of a
150 canonical DCAF substrate receptor.

151   We then crystallised $CDK12^{713-1052}$-$cycK^{1-267}$ bound to CR8 and $DDB1^{\Delta BPB}$ and
152 determined the 3.5 Å resolution structure of this complex (**Fig. 2d**, **Extended Data Table 1**).
153 In the structure, CDK12 forms extensive protein-protein interactions (~2000 $Å^2$) with DDB1.
154 CR8 binds the active site of CDK12 and bridges the CDK12-DDB1 interface, while cycK binds
155 CDK12 on the opposite site and does not contact DDB1. The N- and C-lobes of CDK12 are
156 proximal to DDB1 residues located in a loop of the BPA domain (amino acid (aa) 111-114),
157 BPC-helix 2 (aa 986-990), and a loop in the C-terminal domain (aa 1078-1081) that are
158 otherwise involved in DCAF binding (**Extended Data Fig. 5**). In addition, the C-terminal
159 extension of CDK12 binds the cleft between the DDB1 domains BPA and BPC, a hallmark
160 binding site of DDB1-DCAF interactions (**Extended Data Fig. 5a-d, h**). The density for this
161 region could only be tentatively assigned, likely due to the presence of multiple conformations,
162 but the CDK12 C-terminal tail clearly engages with DDB1 and assumes a conformation
163 different from those seen in isolated CDK12-cycK structures (**Extended Data Fig.
164 6a, b, d**)[19,21]. Structure-guided mutational analyses combined with time-resolved fluorescence
165 resonance energy transfer (TR-FRET) assays was used to assess the contribution of these
166 interactions to CR8-dependent CDK12-DDB1 complex formation (**Fig. 2e and Extended
167 Data Fig. 5e**). CDK12 thus assumes the role of a glue-induced substrate receptor and places
168 cycK in a position that is typically occupied by CRL4 substrates (**Fig. 2f**). This renders CDK12-
169 cycK binding to DDB1 mutually exclusive with that of DCAFs and provides a structural
170 framework for why a canonical substrate receptor is dispensable for cycK ubiquitination.

171

172 **CDK12-DDB1 interface confers selectivity**
173 CR8 is a pleiotropic CDK inhibitor reported to bind CDK1/2/3/5/7/9/12[19,22], yet in cells we
174 observed selective cycK destabilization in the presence of the drug. As cycK is reported to
175 associate with CDK9, CDK12 and CDK13, we tested whether the other cycK-dependent

176   kinases are also recruited to DDB1. The closely related CDK13 (90.8 % sequence identity,

177   **Extended Data Fig. 7a**), but not the more divergent CDK9 (45.5 % sequence identity,

178   **Extended Data Fig. 7b, c**), was recruited to DDB1 in the presence of CR8, albeit with a

179   slightly lower binding affinity (**Extended Data Fig. 7d-f**). Analogously, less productive *in*

180   *vitro* cycK ubiquitination was observed for CDK13 compared to CDK12 (**Extended Data**

181   **Fig. 7g**). The main difference between CDK9 and CDK12/13 primary sequence lies in their C-

182   terminal extension (**Extended Data Fig. 7a, b**), which in our structure nestles up against DDB1

183   BPA and BPC propellers (**Fig. 2d and Extended Data Fig. 5d, h**). Mutations in, or truncation

184   of, the CDK12 C-terminal extension (**Extended Data Fig. 5c**) abolished basal binding between

185   CDK12 and DDB1, whereas complex formation could still be facilitated by CR8 to a varying

186   extent (**Extended Data Fig. 7h, i**). Hence, our data shows that the pan-selective CDK inhibitor

187   CR8 induces specific protein-protein interactions between CDK12/13 and DDB1 and suggest

188   that the C-terminal extension, while contributing to binding, is not essential for drug-dependent

189   kinase recruitment.

190

191   **CR8 phenylpyridine confers glue activity**

192   CR8 occupies the ATP binding pocket of CDK12 and forms discrete contacts with residues in

193   the BPC domain of DDB1 (~150 $Å^2$) through its hydrophobic phenylpyridine ring system (**Fig.**

194   **3a, b**). Mutation of the DDB1 residues Ile909, Arg928, and Arg947 each diminished drug-

195   induced recruitment of the kinase (**Fig. 3c**), highlighting the contribution of the phenylpyridine

196   moiety to complex formation. To evaluate the structure-activity relationship underlying the

197   gain-of-function activity of CR8, we probed other CDK inhibitors for their ability to drive

198   complex formation between DDB1 and CDK12. DRF053[23], a CR8-related inhibitor that carries

199   a differently linked phenylpyridine ring system (**Fig. 3a, d**), induced binding with two-fold

200   lower affinity than CR8 (**Extended Data Fig. 8a**). Roscovitine[24], the parent compound of CR8

201   that lacks the 2-pyridyl substituent but retains the phenyl ring proximal to Arg928 (**Fig. 3a, d**),

202   also facilitated complex formation, albeit with a 3-fold lower apparent affinity (**Extended Data**

203   **Fig. 8a**). The affinity rank-order observed in our TR-FRET assay correlated with the degree of

204   cycK ubiquitination *in vitro*, in which DRF053 and roscovitine showed less processive

205   ubiquitination (**Fig. 3e**). As neither DRF053 nor roscovitine induced degradation of the

206   cycK$_{eGFP}$ reporter in cells (**Fig. 3f**), our results demonstrate that the presence and correct

207   orientation of the 2-pyridyl on the surface of CDK12 confer the gain-of-function activity of

208   CR8 leading to cycK degradation.

209   To test whether any ligand could in principle drive the interaction of CDK12 with

210   DDB1, we tested the endogenous CDK nucleotide cofactor ATP for its ability to promote

211   complex formation. ATP neither facilitated nor abrogated the interaction over basal binding

212   observed in the presence of DMSO (**Extended Data Fig. 6c**), suggesting that although the

213   nucleotide-bound conformation of CDK12 seems incompatible with approaching DDB1

214   (**Extended Data Fig. 6b**), its C-terminal extension is free to adopt multiple conformations[21].

215   THZ531[25], a bulky covalent CDK12/13 inhibitor predicted to clash with DDB1(**Extended**

216   **Data Fig. 6d, e**), locks the CDK12 C-terminal extension in a conformation incompatible with

217   DDB1 recruitment (**Extended Data Fig. 6d**). Consistently, THZ531 further decreased the TR-

218   FRET signal and diminished cycK ubiquitination *in vitro* below DMSO control levels (**Fig. 3e**

219   **and Extended Data Fig. 6c**)[25]. Flavopiridol[26], a natural product-derived inhibitor structurally

220   distinct from CR8 (**Fig. 3a, d**), also stimulated the binding of CDK12-cycK to DDB1

221   (**Extended Data Fig. 8a**). While flavopiridol gave rise to moderate cycK ubiquitination *in vitro*

222   (**Fig. 3e**), it failed to degrade cycK in cells (**Fig. 3f**). Our results thus show that the interactions

223   between the compound and DDB1 display a significant plasticity and that structurally diverse

224   surface-exposed moieties in CR8, DRF053, roscovitine and flavopiridol can facilitate CDK12-

225   cycK recruitment. Small differences in their ability to stabilise the DDB1-CDK12 complex

226   translate, in an almost binary fashion, into cellular degradation of cycK or lack thereof. This

227   behaviour is reminiscent of CRL4[CRBN] and thalidomide analogues[8,27], where an apparent

228   affinity threshold must be overcome to drive drug-induced target degradation.

229

CycK degradation adds to CR8 toxicity

231   Finally, to delineate the contribution of CRL4-mediated cycK degradation to the cellular

232   cytotoxicity of CR8 over non-degradative CDK inhibition, we compared compound toxicity in

233   wild-type HEK293T$_{Cas9}$ cells to cells that were pre-treated with MLN4924 (NEDD8-activating

234   enzyme inhibitor), genetically-depleted for DDB1, or subject to DCAF overexpression. Global

235   inhibition of CRL activity by MLN4924 had only minor effects on cell viability (**Extended**

236   **Data Fig. 9a**), but resulted in decreased sensitivity to CR8 (**Fig. 4a**), showing that CRL

237   neddylation significantly contributes to CR8 toxicity. Overexpression of the substrate receptor

238   CRBN also affected sensitivity to CR8 and decreased cycK degradation (**Fig. 4b, c and**

239   **Extended Data Fig. 9 c-e**), presumably by reducing the free pool of DDB1**.** As expected, CR8-

240   induced endogenous cycK degradation was dependent on DDB1 (**Fig. 4d**) and, consistently,

241   we found that cytotoxicity of CR8, but not that of the other CDK inhibitors, was ten-fold lower

242   in cells depleted for DDB1 (**Fig. 4e and Extended Data Fig. 9f**). Together, this data

243 demonstrates that the CLR4-dependent gain-of-function glue degrader activity of CR8 strongly
244 contributes to its cellular potency and provides an additional layer of ortholog-specific CDK
245 inactivation through cycK degradation.
246

DISCUSSION

Kinase inhibitors have long been suspected to have a degradation component to their mode of action[28,29], and our work provides the first characterization and structural dissection of how a kinase inhibitor scaffold acquires degrader properties. Small molecule glue degraders have thus far only been shown to target substrate-recruiting E3 ligase modules. CDK12 is not a constitutive E3 ligase component, but instead serves as a drug-induced substrate receptor, linking DDB1 to the ubiquitination target, bypassing the requirement for a canonical DCAF. While cycK is the primary ubiquitination target, CDK12 may become subject to autoubiquitination upon prolonged compound exposure similar to canonical DCAFs[30,31]. As CR8 binds the active site of CDK12 and does not require a ligandable pocket on the ligase, developing target-based glue degraders to essential ligase components such as DDB1 could greatly expand the repertoire of ubiquitin ligases accessible to targeted protein degradation. Furthermore, as kinase inhibitors often show poor target selectivity, small molecule-induced kinase inactivation that leverages specific protein-protein interactions could offer a path towards improved drug selectivity and may facilitate the pursuit of CDK12 as an emerging therapeutic target[32].

The gain-of-function glue degrader activity of CR8 is attributed to a 2-pyridyl moiety exposed on the kinase surface. Surface-exposed single residue mutations have been shown to promote higher-order protein assemblies, as the haemoglobin Glu to Val mutation, for example, induces polymerization in sickle cell anaemia[33]. Accordingly, single residue mutations designed to increase surface hydrophobicity give rise to ordered protein aggregates[34,35]. Bound compounds, such as enzyme inhibitors, can in principle mimic such amino acid changes with dramatic effects on the protein interaction landscape, suggesting that compound-induced protein-protein interactions may be more common than previously recognised. Taken together, our results suggest that modifications of surface-exposed regions in target-bound small molecules offer a rational strategy to develop molecular glue degraders for a given protein target.

**Main References**

276

277   1.   Stanton, B. Z., Chory, E. J. & Crabtree, G. R. Chemically induced proximity in
278   biology and medicine. *Science* **359**, (2018).
279   2.   Salami, J. & Crews, C. M. Waste disposal - An attractive strategy for cancer therapy.
280   *Science* **355** 1163–1167 (2017).
281   3.   Chopra, R., Sadok, A. & Collins, I. A critical evaluation of the approaches to targeted
282   protein degradation for drug discovery. *Drug Discov. Today Technol.* **31**, 5–13 (2019).
283   4.   Fink, E. C. & Ebert, B. L. The novel mechanism of lenalidomide activity. *Blood* **126**,
284   2366–2369 (2015).
285   5.   Lu, G. *et al.* The myeloma drug lenalidomide promotes the cereblon-dependent
286   destruction of ikaros proteins. *Science* **343**, 305–309 (2014).
287   6.   Krönke, J. *et al.* Lenalidomide causes selective degradation of IKZF1 and IKZF3 in
288   multiple myeloma cells. *Science* **343**, 301–305 (2014).
289   7.   Matyskiela, M. E. *et al.* A novel cereblon modulator recruits GSPT1 to the CRL4
290   CRBN ubiquitin ligase. *Nature* **535**, 252–257 (2016).
291   8.   Petzold, G., Fischer, E. S. & Thomä, N. H. Structural basis of lenalidomide-induced
292   CK1α degradation by the CRL4 CRBN ubiquitin ligase. *Nature* **532**, 127–130 (2016).
293   9.   Fischer, E. S. *et al.* Structure of the DDB1-CRBN E3 ubiquitin ligase in complex with
294   thalidomide. *Nature* **512**, 49–53 (2014).
295   10.   Han, T. *et al.* Anticancer sulfonamides target splicing by inducing RBM39 degradation
296   via recruitment to DCAF15. *Science* **356**, 3755 (2017).
297   11.   Uehara, T. *et al.* Selective degradation of splicing factor CAPERα by anticancer
298   sulfonamides. *Nat. Chem. Biol.* **13**, 675–680 (2017).
299   12.   Faust, T. B. *et al.* Structural complementarity facilitates E7820-mediated degradation
300   of RBM39 by DCAF15. *Nat. Chem. Biol.* (2019) doi:10.1038/s41589-019-0378-3.
301   13.   Bondeson, D. P. *et al.* Catalytic in vivo protein knockdown by small-molecule
302   PROTACs. *Nat. Chem. Biol.* **11**, 611–617 (2015).
303   14.   Yu, C. *et al.* High-throughput identification of genotype-specific cancer vulnerabilities
304   in mixtures of barcoded tumor cell lines. *Nat. Biotechnol.* **34**, 419–423 (2016).
305   15.   Corsello, S. M. *et al.* Non-oncology drugs are a source of previously unappreciated
306   anti-cancer activity. *Biorxiv* (2019) doi:10.1101/730119.
307   16.   Ghandi, M. *et al.* Next-generation characterization of the Cancer Cell Line
308   Encyclopedia. *Nature* **569**, 503–508 (2019).
309   17.   Angers, S. *et al.* Molecular architecture and assembly of the DDB1-CUL4A ubiquitin
310   ligase machinery. *Nature* **443**, 590–593 (2006).
311   18.   Lee, J. & Zhou, P. DCAFs, the Missing Link of the CUL4-DDB1 Ubiquitin Ligase.
312   *Mol. Cell* **26**, 775–780 (2007).
313   19.   Bösken, C. A. *et al.* The structure and substrate specificity of human Cdk12/Cyclin K.
314   *Nat. Commun.* **5**, (2014).
315   20.   Li, T., Chen, X., Garbutt, K. C., Zhou, P. & Zheng, N. Structure of DDB1 in Complex
316   with a Paramyxovirus V Protein: Viral Hijack of a Propeller Cluster in Ubiquitin
317   Ligase. *Cell* **124**, 105–117 (2006).
318   21.   Dixon-Clarke, S. E., Elkins, J. M., Cheng, S. W. G., Morin, G. B. & Bullock, A. N.
319   Structures of the CDK12/CycK complex with AMP-PNP reveal a flexible C-terminal
320   kinase extension important for ATP binding. *Sci. Rep.* **5**, (2015).
321   22.   Bettayeb, K. *et al.* CR8, a potent and selective, roscovitine-derived inhibitor of cyclin-
322   dependent kinases. *Oncogene* **27**, 5797–5807 (2008).
323   23.   Oumata, N. *et al.* Roscovitine-Derived, Dual-Specificity Inhibitors of Cyclin-
324   Dependent Kinases and Casein Kinases 1. *J. Med. Chem.* **51**, 5229–5242 (2008).
325   24.   Meijer, L. *et al.* Biochemical and Cellular Effects of Roscovitine, a Potent and

326   Selective Inhibitor of the Cyclin-Dependent Kinases cdc2, cdk2 and cdk5. *Eur. J.*
327   *Biochem.* **243**, 527–536 (1997).

328   25.   Zhang, T. *et al.* Covalent targeting of remote cysteine residues to develop CDK12 and
329   CDK13 inhibitors. *Nat. Chem. Biol.* **12**, 876–884 (2016).

330   26.   Sedlacek, H. H. *et al.* Flavopiridol (L86 8275; NSC 649890), a new kinase inhibitor
331   for tumor therapy. *Int. J. Oncol.* **9**, 1143–1168 (1996).

332   27.   Sievers, Q. L. *et al.* Defining the human C2H2 zinc finger degrome targeted by
333   thalidomide analogs through CRBN. *Science* **362**, (2018).

334   28.   Jones, L. H. Small-Molecule Kinase Downregulators. *Cell Chem. Biol.* **25**, 30–35
335   (2018).

336   29.   Schreiber, S. L. A chemical biology view of bioactive small molecules and a binder-
337   based approach to connect biology to precision medicines. *Israel Journal of Chemistry*
338   **59** 52–59 (2019).

339   30.   Ito, T. *et al.* Identification of a primary target of thalidomide teratogenicity. *Science*
340   **327**, 1345–1350 (2010).

341   31.   Fischer, E. S. *et al.* The molecular basis of CRL4DDB2/CSAubiquitin ligase
342   architecture, targeting, and activation. *Cell* **147**, 1024–1039 (2011).

343   32.   Johnson, S. F. *et al.* CDK12 Inhibition Reverses De Novo and Acquired PARP
344   Inhibitor Resistance in BRCA Wild-Type and Mutated Models of Triple-Negative
345   Breast Cancer. *Cell Rep.* (2016) doi:10.1016/j.celrep.2016.10.077.

346   33.   Dykes, G. W., Crepeau, R. H. & Edelstein, S. J. Three-dimensional reconstruction of
347   the 14-filament fibers of hemoglobin S. *J. Mol. Biol.* **130**, 451–72 (1979).

348   34.   Levy, E. D. A simple definition of structural regions in proteins and its use in
349   analyzing interface evolution. *J. Mol. Biol.* **403**, 660–670 (2010).

350   35.   Garcia-Seisdedos, H., Empereur-Mot, C., Elad, N. & Levy, E. D. Proteins evolve on
351   the edge of supramolecular self-assembly. *Nat. Publ. Gr.* **548**, (2017).

352
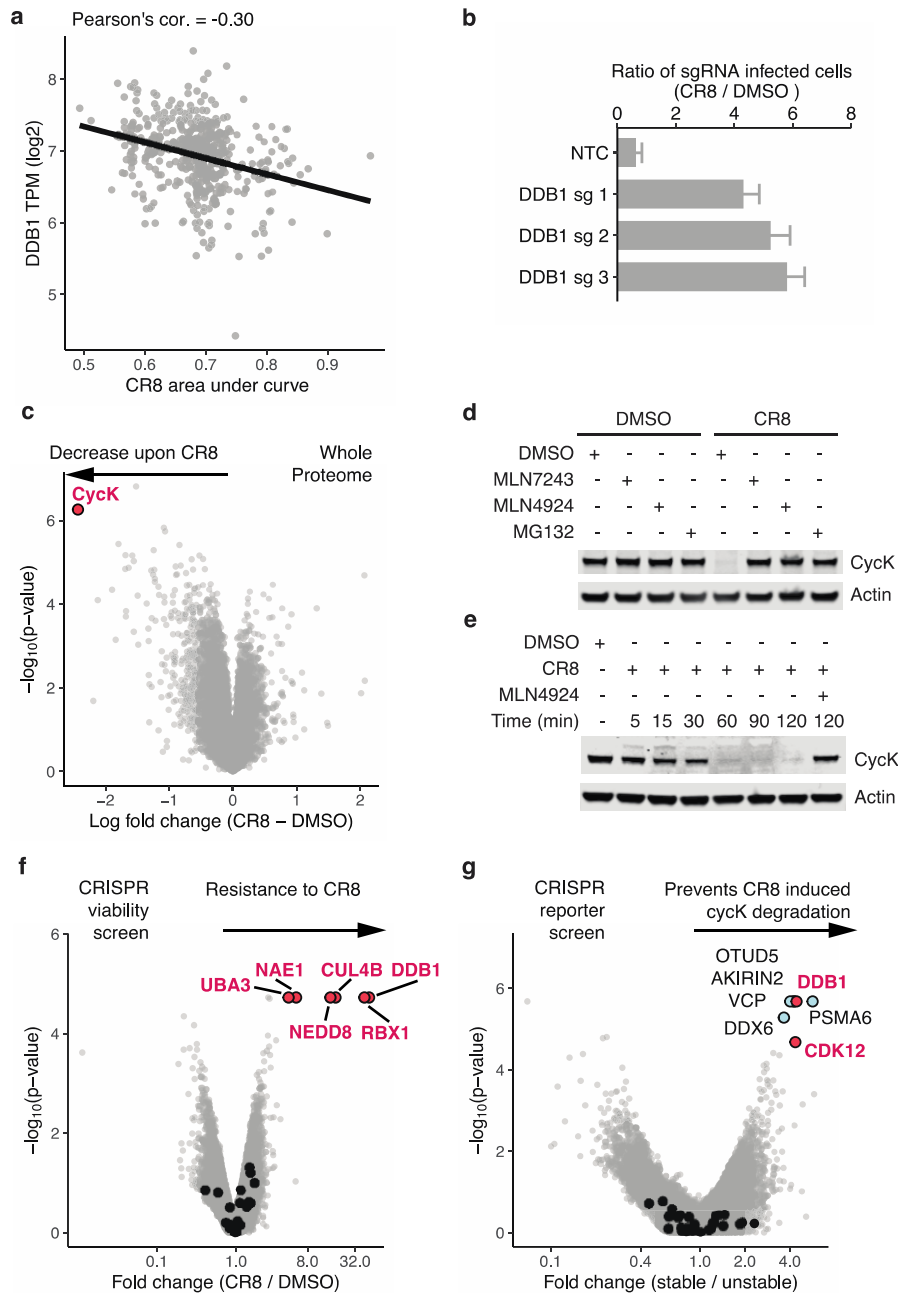
Figure 1 | CR8-induced degradation of cycK depends on DDB1 and CDK12. a, Correlation between CR8 toxicity and mRNA expression of DDB1 in 578 cancer cell lines. Lower area under the curve (AUC) corresponds to higher drug toxicity. TPM, transcripts per million. **b**, HEK293T$_{Cas9}$ cells were transduced with BFP (blue fluorescent protein) labelled sgRNAs, treated with DMSO or 1 µM CR8 and analysed by flow cytometry. Data represent the mean ± s.d. (n=3). **c**, Molt-4 cells were exposed to 1 µM CR8 or DMSO for 5 hours followed by whole proteome quantification using tandem mass tag mass spectrometry (mean log2 fold change, p value calculated by a moderated t-test, n=3 (DMSO), n=1 (CR8). **d**, HEK293T$_{Cas9}$ cells were treated with DMSO, 0.5 µM MLN7243 (ubiquitin activating enzyme inhibitor), 1 µM MLN4924 (NEDD8-activating enzyme inhibitor), or 10 µM MG132 (proteasome inhibitor) for 2 hours followed by exposure to 1 µM CR8 for 2 hours. Lysates were immunoblotted for the indicated targets (n=3, representative image shown). **e**, HEK293T$_{Cas9}$ cells were treated with DMSO or 1 µM MLN4924 for 2 hours followed by exposure to 1 µM CR8 (n=3, representative image shown). **f**, Median fold change of read counts (CR8/DMSO treatment) and corresponding p values (empirical rank-sum test-statistic) for single guide RNAs (sgRNAs) targeting 19,112 human genes conferring resistance to CR8 treatment. DCAF substrate receptors are labelled with black dots (n=1). **g**, Median

370   fold change of read counts (cycK stable/unstable) and corresponding p values (empirical rank-sum test-
371   statistic) for sgRNAs targeting 19,112 human genes preventing CR8 induced cycK$_{eGFP}$ degradation.
372   DCAF substrate receptors are labelled with black dots (n=3).
373
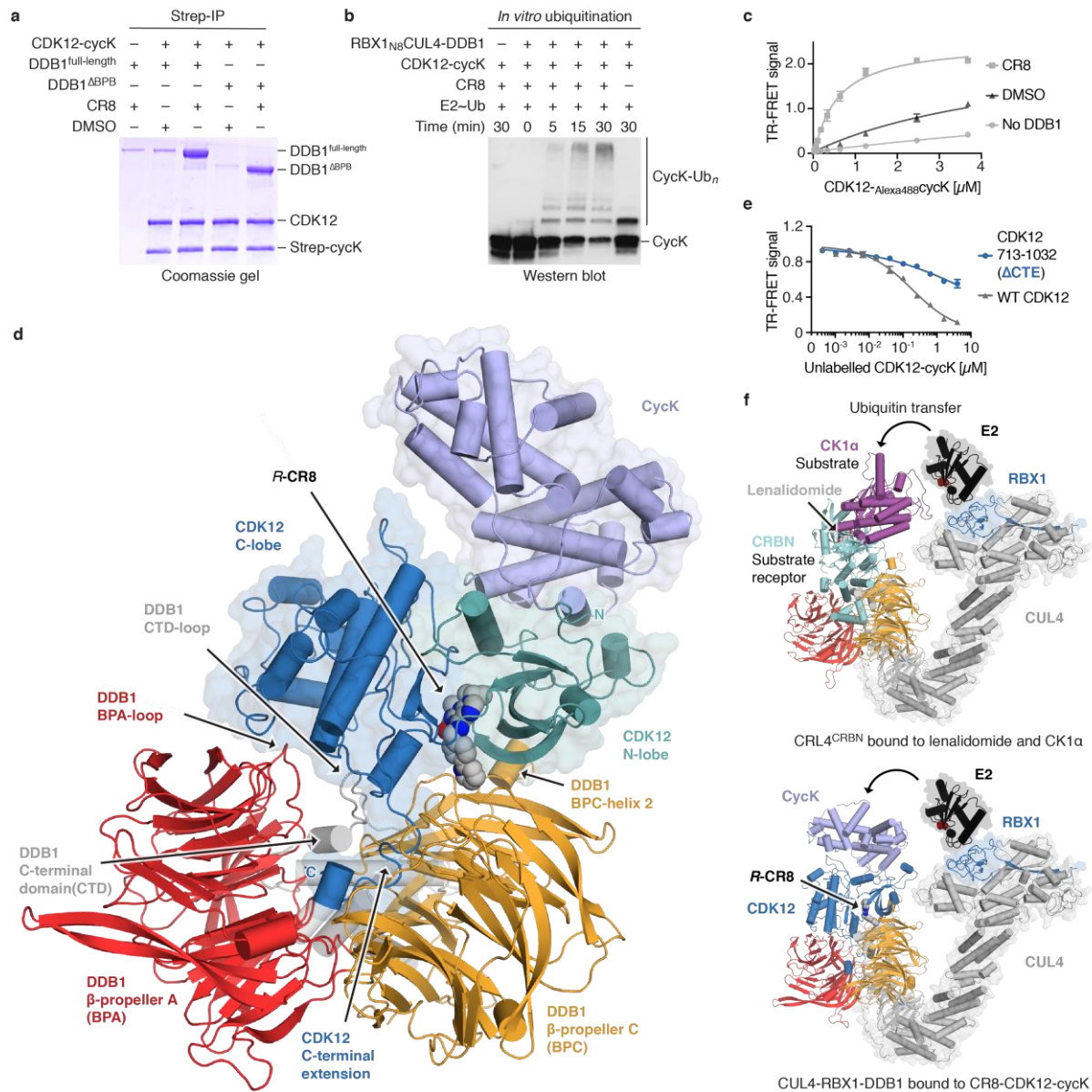
Figure 2 | CR8-bound CDK12 interacts with DDB1 in a DCAF-like manner. a, Co-immunoprecipitation (IP) experiments with recombinant proteins. **b**, *In vitro* ubiquitination of cycK by the RBX1$_{N8}$CUL4-DDB1 ubiquitin ligase core. **c**, TR-FRET signal for CDK12-$_{Alexa488}$cycK titrated to $_{Terbium}$DDB1 in DMSO or 10 μM CR8. The no DDB1 control contains streptavidin-terbium and shows concentration-dependent fluorophore effects. Data represent the mean ± s.d. (n=3). **d**, Cartoon representation of the DDB1^{ΔBPB}-*R*-CR8-CDK12-cycK crystal structure. **e**, TR-FRET counter titration of unlabelled wild-type or mutant CDK12-cycK (0-10 μM) into pre-assembled $_{Terbium}$DDB1-CR8-CDK12-$_{Alexa488}$cycK complex. Data represent the mean ± s.d. (n=3). **f**, Structural models of CRL4^{CRBN} bound to lenalidomide and CK1alpha (top) and RBX1-CUL4-DDB1 (CRL4) bound to the *R*-CR8-CDK12-cycK complex (bottom). The active site cysteine of the E2 enzyme (red spheres) provides ubiquitin through a thioester bond.

15
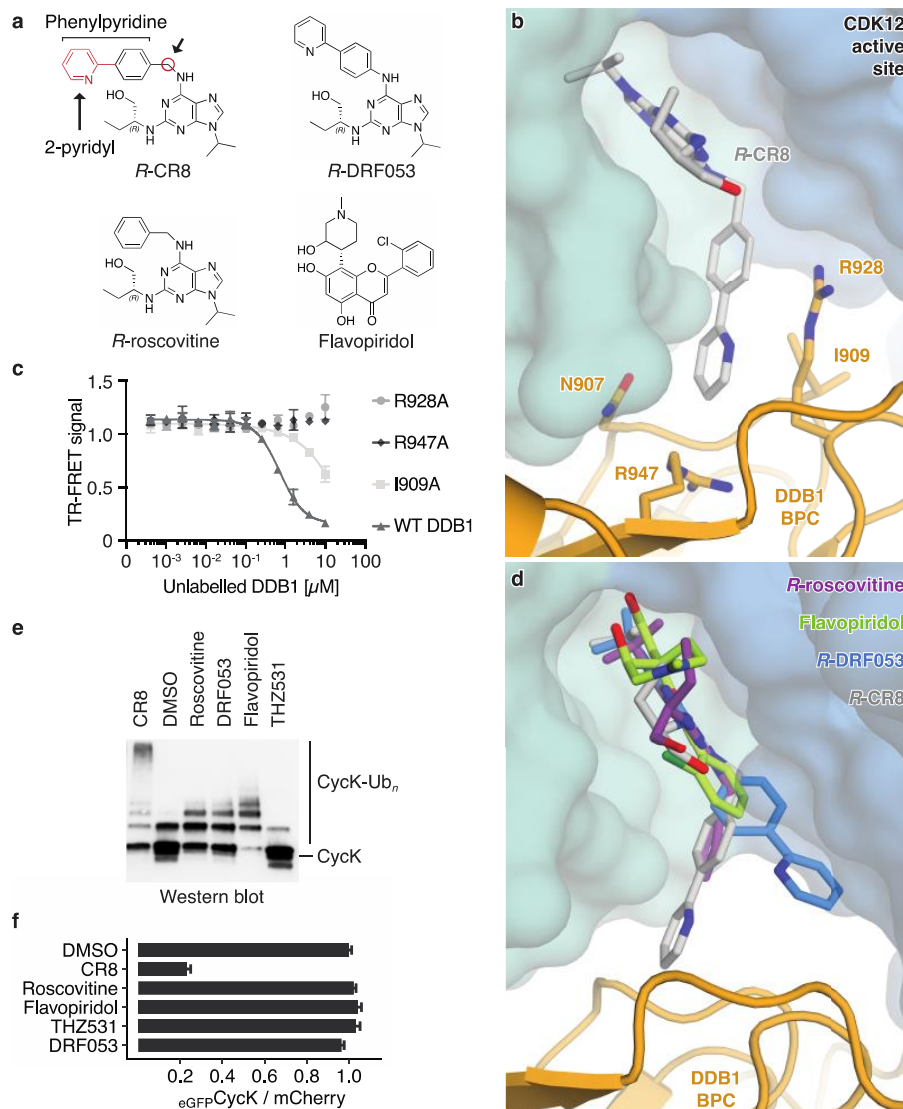
388
389 **Figure 3 | Molecular glue degrader activity of CR8 is conferred by a surface-exposed 2-pyridyl**
390 **moiety. a**, Chemical structures of *R*-CR8, *R*-DRF053, *R*-roscovitine and flavopiridol. Arrows indicate
391 differences between *R*-CR8, *R*-DRF053 and *R*-roscovitine. **b**, Close-up of the CDK12-CR8-DDB1
392 interface. The phenylpyridine moiety of CR8 contacts DDB1 residues. **c**, Titration of unlabelled wild-
393 type or mutant DDB1 (0-10 µM) into pre-assembled $_{Terbium}$DDB1-CR8-CDK12-$_{Alexa488}$cycK complex.
394 Data represent the mean ± s.d. (n=3). **d**, *R*-roscovitine (PDB entry 2A4L), *R*-DRF053 and flavopiridol
395 (PDB entry 3BLR) in the active site of CDK12 in the DDB1-CR8-CDK12-cycK complex through
396 superposition of the respective kinase domains or the purine moiety (in case of DRF053). **e**, *In vitro*
397 ubiquitination of CDK12-cycK complex by RBX1$_{N8}$CUL4-DDB1 in the absence (DMSO) or presence
398 of 2 µM compound. **f**, CycK$_{eGFP}$ HEK293T$_{Cas9}$ cells were treated with 1 µM of the indicated compound
399 for 2 hours and analysed by flow cytometry. Data represent the mean ± s.d. (n=3).
400
401

16
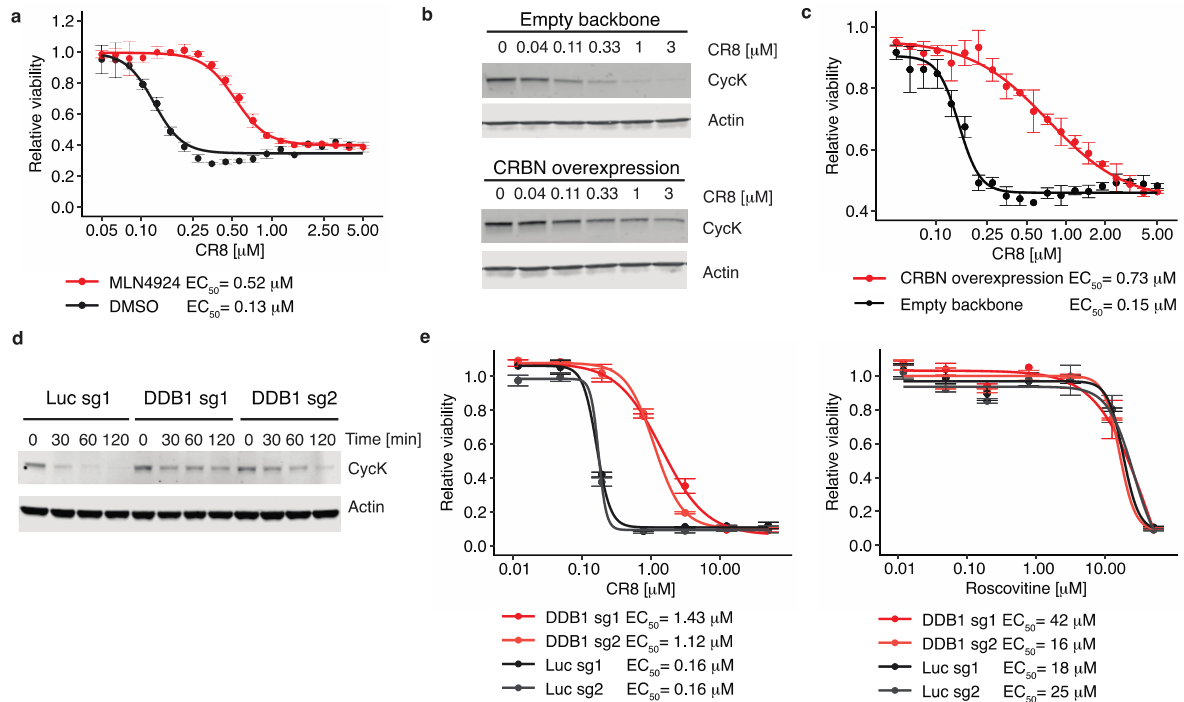
Figure 4 | CR8-mediated cycK degradation contributes to its cellular potency. a, HEK293T$_{Cas9}$ cells were exposed to DMSO or 100 nM MLN4924 at indicated concentrations of CR8 for 3 days. This dose of MLN4924 alone did not influence cell viability (Extended Data Fig. 9a). Data represent mean ± s.d. Lines represent standard four-parameter log-logistic curves (n=3). **b**, HEK293T$_{Cas9}$ cells were transiently transfected with control or CRBN overexpression vectors and after 48h lysates were immunoblotted for the indicated targets. **c**, HEK293T$_{Cas9}$ cells were transiently transfected with control or CRBN overexpression vectors and after 48h were exposed to the indicated concentration of CR8 for 3 days. Data represent mean ± s.d. Lines represent standard four-parameter log-logistic curves (n=3). **d**, HEK293T$_{Cas9}$ cells were transfected with a fluorophore and sgRNAs targeting DDB1 or a non-targeting control (NTC) and exposed to CR8 for the indicated time. Protein lysates were immunoblotted for the indicated targets (n=2, representative image shown). **e**, HEK293T$_{Cas9}$ cells were transduced with sgRNAs targeting DDB1 or luciferase and exposed to the indicated concentration of CR8, roscovitine, or DMSO for 3 days. Data represent mean ± s.d. Lines represent standard four-parameter log-logistic curves (n=3).

418 **Methods**
419
420 **Mammalian cell culture**

421 The human HEK293T cell lines were provided by the Genetic Perturbation Platform, Broad

422 Institute and K562$_{Cas9}$, THP1$_{Cas9}$, P31FUJ$_{Cas9}$ cell lines were provided by Zuzana Tothova,

423 Broad Institute and HEK293T$_{Cas9}$[27] and MM1S$_{Cas9}$[36] were previously published. HEK293T

424 cells were cultured in DMEM (Gibco) and all other cell lines in RPMI (Gibco), with 10% FBS

425 (Invitrogen), glutamine (Invitrogen) and penicillin–streptomycin (Invitrogen) at 37 °C and 5%

426 CO_2.

427

428 **Compounds**

429 *R*-CR8 (3605) was obtained from Tocris, *S*-CR8 (ALX-270-509-M005), flavopiridol (ALX-

430 430-161-M005) from Enzo Life Sciences, roscovitine (HY-30237), THZ531 (HY-103618),

431 LDC00067 (HY-15878) from MedChem Express and DRF053 (D6946-5MG) from Sigma.

432

433 **Antibodies**

434 The following antibodies were used in this study: anti-cycK (Bethyl Laboratories, A301-939A

435 for full length cycK), anti-cycK (abcam, ab251652, for cycK$^{1-267}$), anti-beta-actin (Cell

436 Signaling, #3700), anti-mouse 800CW (LI-COR Biosciences, 926-32211), anti-rabbit 680LT

437 (LI-COR Biosciences, 925-68021), anti-rabbit IgG antibodies (abcam, ab6721).

438

439 **Reporter vectors**

440 The following reporter were used in this study: Artichoke (SFFV.BsmBICloneSite-

441 17aaRigidLinker-eGFP.IRES.mCherry.cppt.EF1α.PuroR, Addgene #73320 for Genome wide

442 screen and validation experiments), Cilantro 2 (PGK.BsmBICloneSite-10aaFlexibleLinker-

443 eGFP.IRES.mCherry. cppt.EF1α.PuroR, Addgene #74450 for degradation kinetics), sgBFP

444 (sgRNA.SFFV.tBFP, for Validation of drug-E3 ligase pairs), sgRFP657,

445 (sgRNA.EFS.RFP657 for Validation of drug-E3 ligase pairs), sgPuro, (pXPR003, Addgene

446 #52963, for drug sensitivity assays).

447

448 **Oligos**

449 List of all oligonucleotides used in this study can be found in Supplementary Oligo Table 1.

450

451 **Bioinformatic screen**

We computed Pearson correlations of viability of PRISM repurposing compounds in 8 doses and 578 cell lines[15] with gene expression (GE) and copy number variation (CN) of all detectable protein-coding genes of matched cell lines from The Cancer Cell Line Encyclopedia (CCLE)[16]. Z score was computed for each pair of compounds, dose viability, and genomic feature (GE or CN) across all cell lines. For each compound-genomic feature pair, the most extreme correlations are ranked from negative to positive. To focus on novel compound-gene relationships, we restricted genes to a curated list of 499 E3 ligase components and compounds that are not one of "EGFR inhibitor", "RAF inhibitor" or "MDM inhibitor" based on PRISM repurposing annotation[16]. Hit compounds were selected if either the Z score was less than -6 or ranked in the top 15 with Z score less than -4. The resulting list of 158 E3 gene-compound pairs was further curated and shortened manually to 96 E3 gene-compound pairs, which included 95 unique E3 ligases and 85 unique compounds.

Cloning and lentiviral packaging of sgRNAs targeting 95 E3 ligases

sgRNAs targeting E3 ligases were selected from the human Brunello CRISPR library[37]. 170 oligo pairs (IDT) targeting 95 E3 ligases were annealed and cloned into the sgRNA.SFFV.tBFP (Guide ID A) or sgRNA.EFS.RFP657 (Guide ID B) fluorescent vectors in a 96-well format using previously published protocols[38]. Briefly, vectors were linearized with BsmBI (New England Biolabs) and gel purified with the Spin Miniprep Kit (Qiagen). Annealed oligos were phosphorylated with T4 Polynucleotide Kinase (New England Biolabs) and ligated into the linearized and purified vector backbones with T4 DNA Ligase (New England Biolabs). Constructs were transformed into XL10-Gold ultracompetent *Escherichia coli* (Stratagene/Agilent Technologies), plasmids were purified using MiniPrep Kit (Qiagen), and guide sequence confirmed by Sanger sequencing. For validation of the primary screen, virus was produced in a 96-well format. Briefly, 11,000 HEK293T cells were seeded per well in 100 µL DMEM medium supplemented with 10% FBS and Penicillin-Streptomycin-Glutamine. The next day a Packaging Mix was prepared in a 96-well plate consisting of 500 ng psPAX2, 50 ng pVSV-G and 17 ng sgRNA backbone in 5 µL OptiMem (Invitrogen) and incubated for 5 minutes at room temperature. This mix was combined with 0.1 µL TransIT-LT1 (Mirus) in 5 µL of OptiMem, incubated for 30 minutes at room temperature, and then applied to cells. Two days post-transfection, dead cells were removed by centrifugation and lentivirus containing medium was collected stored at -80°C prior to use.

Validation of drug-E3 ligase pairs from the bioinformatic screen

486 K562$_{Cas9}$, OVK16$_{Cas9}$, A564$_{Cas9}$, ES2$_{Cas9}$ and MOLM13$_{Cas9}$ cell lines were individually

487 transduced with 192 sgRNAs targeting 95 E3 ligases in a 96-well plate format. 3000 cells/well

488 were plated in 100 µL RPMI supplemented with 10% FCS and Penicillin-Streptomycin-

489 Glutamine and 30µL/well of virus supernatant was added. 24 hours post infection the medium

490 was changed. After three days, the percentage of sgRNA transduced cells was determined by

491 flow cytometry. If more than 60% of cells were transduced, un-transduced cells were added to

492 bring the level below 60%. Eight days post-infection cell density was measured and adjusted

493 to 1.5 x 10^5 cells/mL with RPMI. For treatment, 50 µL of sgRNA transduced cells were seeded

494 into each well of a 384 well plate with pre-plated DMSO or cognate drug in three

495 concentrations (0.1 µM, 1 µM, 10 µM) with Agilent BRAVO Automated Liquid Handling

496 Platform. Plates were sealed with White Rayon adhesive sealing tape (Thermo Fisher

497 Scientific) and grown for three days. Adherent cell lines were trypsinised and re-suspended in

498 50 µL of RPMI with Matrix WellMate (Thermo Scientific). Suspension cells were directly

499 subjected to analysis. 10 µL of cell suspension was subjected to the flow analysis with

500 FACSCanto equipped with High Throughput Sampler (BD Bioscience). The percentage of

501 sgRNA transduced cells in the drug treatment wells was normalised to the DMSO control.

502 Wells with fluorescent drug and samples with less than 120 viable cells events or less than 6%

503 fluorescent cells were removed from analysis. All E3-drug pairs were ranked based on the

504 number of experimental conditions (cell line and drug dose) with more than 50% of sgRNA

505 transduced cells in drug treatment wells in comparison to corresponding DMSO control.

506

Validation of DDB1 resistance phenotype

508 For validation experiments, virus was produced in a 6-well plate format, as described above

509 with the following adjustments: 2.5 x 10^5 HEK293T cells/well in 2 mL DMEM medium, 3

510 µL/well of TransIT-LT1, 15 µL/well of OPTI-MEM, 500 ng/well of the desired plasmid,

511 500 ng/well psPAX2, and 50 ng/well pVSV-G in 32.5 µL/well OPTI-MEM. After collecting

512 the virus, 10 x 10^3 HEK293T$_{Cas9}$ cells in 100 µL DMEM medium were transduced with 10 µL

513 of virus supernatant. The transduced HEK293T$_{Cas9}$ cells were then mixed with untransduced

514 control cells at a 1:9 ratio. Nine days after sgRNA transduction, cells were treated for 3 days

515 with DMSO or 1 µM CR8 and analysed by flow cytometry to determine the percentage of

516 BFP$^+$ cells. sgRNAs targeting DDB1 provide partial depletion of DDB1 (50% DDB1 alleles

517 modified, reducing DDB1 levels by roughly 50%), which suggests selection towards

518 heterozygous or hypomorphic clones.

519

Whole proteome quantification using tandem mass tag mass spectrometry

10×10^6 Molt-4 cells were treated with DMSO (triplicate) or 1 µM CR8 (single replicate) for 1 or 5 hours and later were harvested by centrifugation. Samples were processed, measured and analysed as described before[39]. Data are available in the PRIDE repository (PXD016187 and PXD016188).

Quantitative PCR

HEK293T$_{Cas9}$ cells were treated with DMSO or 1 µM CR8 for 2 hours, collected by centrifugation, washed with PBS, and snap-frozen at -80°C. mRNA was isolated using a QIAGEN RNA kit (Qiagen, 74106). For cDNA synthesis, total RNA was reverse transcribed using a High-Capacity cDNA Reverse Transcription Kit (Thermo Fischer) before qPCR analysis with TaqMan Fast Advanced Master Mix (ThermoFisher Scientific, 4444557) for CCNK (TaqMan, Hs00171095_m1, Life Technologies) and GAPDH (TaqMan, Hs02758991_g1). Reactions were run and analysed on a CFX96 Real Time system (Bio-Rad).

Immunoblots for whole protein lysate

Cells were washed with phosphate buffered saline (PBS) and lysed (150 mM NaCl, 50 mM Tris (pH 7.5), 1% NP-40, 1% glycerol, 1x Halt Cocktail protease and phosphatase inhibitors) for 20 minutes on ice. The insoluble fraction was removed by centrifugation, protein concentration was quantified using a BCA protein assay kit (Pierce), and equal amount of lysate was run on SDS-PAGE 4-12% Bis-Tris Protein Gels (NuPAGE, Thermo Fisher) and subsequently transferred to nitrocellulose membrane with Trans-Blot Turbo System (BIO-RAD). Membranes were blocked in Odyssey Blocking Buffer/PBS (LI-COR Biosciences) and incubated with primary antibodies overnight at 4°C. The membranes were then washed in TBS-T, incubated for 1 hour with secondary IRDye-conjugated antibodies (LI-COR Biosciences), and washed three times in TBS-T for 5 minutes prior to Near-Infrared Western blot detection on an Odyssey Imaging System (LI-COR Biosciences).

CycK stability reporter analysis

HEK293T$_{Cas9}$ expressing the cycK$_{eGFP}$ degradation reporter were transduced with experimental sgRNAs. Nine days after infection the cells were dosed for 2 hours with DMSO or 1 µM CR8. Using FLOWJO (flow cytometry analysis software), the geometric mean of eGFP and mCherry fluorescent signal for round and mCherry positive cells was calculated. The ratio of eGFP to mCherry was normalised to the average of three DMSO-treated controls.

554

Genome wide CRISPR – CR8 resistance screen

5% (v/v) of the human genome-wide CRISPR-KO Brunello library with 0.4 µL Polybrene/mL (stock of 8 mg/mL) was added to 1.5 x 10^8 HEK293T$_{Cas9}$ in 75 mL of medium and transduced (2400 rpm, 2 hours, 37°C). 24h after infection sgRNA transduced cells were selected with 2 µg/mL of Puromycin for two days. On the ninth day post-infection, cells were treated with either DMSO or 1 µM CR8 and cultured for an additional 3 days. Resistant live cells were selected by gently washing away detached dead cells from the medium. Cell pellets were resuspended in multiple direct lysis buffer reactions (1 mM $CaCl_2$, 3 mM $MgCl_2$, 1 mM EDTA, 1% Triton X-100, Tris pH 7.5 - with freshly supplemented 0.2 mg/mL Proteinase) with 1x10^6 cells per 100 µL reaction. The sgRNA sequence was amplified in a first PCR reaction with eight staggered forward primers. 20 µL of direct lysed cells was mixed with 0.04U Titanium Taq (Takara Bio 639210), 0.5 x Titanium Taq buffer, 800 µM dNTP mix, 200 nM SBS3-Stagger-pXPR003 forward primer, 200 nM SBS12-pXPR003 reverse primer in a 50 µL reaction (cycles: 5 minutes at 94°C, 15 x (30 sec at 94°C, 15 sec at 58°C, 30 sec at 72°C), 2 minutes at 72°C). 2 µL of the first PCR reaction was used as the template for 15 cycles of the second PCR, where Illumina adapters and barcodes were added (0.04U Titanium Taq, 1 x Titanium Taq buffer, 800 µM dNTP mix, 200 nM

P5-SBS3 forward primer, 200 nM P7-barcode-SBS12 reverse primer). An equal amount of all samples was pooled and subjected to preparative agarose electrophoresis followed by gel purification (Qiagen). Eluted DNA was further purified by NaOAc and isopropanol precipitation. Amplified sgRNAs were quantified using Illumina NextSeq platform. Read counts for all guides targeting the same gene were used to generate p-values. Hits enriched in resistance population with False Discovery Rate (FDR) < 0.05 and enriched > 5-fold, are labelled on the plot (Fig. 1f)[40].

BISON CRISPR – CR8 resistance screen

The BISON CRISPR library targets 713 E1, E2, and E3 ubiquitin ligases, deubiquitinases, and control genes and contains 2,852 guide RNAs. It was cloned into the pXPR003 as previously described[37] by the Broad Institute Genome Perturbation Platform (GPP). The virus for the library was produced in a T-175 flask format, as described above with the following adjustments: 1.8 x 10^7 HEK293T cells in 25 mL complete DMEM medium, 244 µL of TransIT-LT1, 5 mL of OPTI-MEM, 32 µg of library, 40 µg psPAX2, and 4 µg pVSV-G in 1 mL OPTI-MEM. 10% (v/v) of BISON CRISPR library was added to 6 x 10^6 HEK293T$_{Cas9}$ cells in

588   triplicates and transduced. Samples were processed as describe above for the genome wide

589   resistance screen.

590

Genome wide CRISPR – cycK stability reporter screen

592   A single clone of cycK$_{eGFP}$ HEK293T$_{Cas9}$ was transduced with the genome wide Brunello

593   library as described above with the following modification: 4.5 x 10^8 cycK$_{eGFP}$ HEK293T$_{Cas9}$

594   cells in 225 mL of medium. Nine days later cells were treated with CR8 or DMSO for at least

595   2 hours and the cycK stable population was separated using fluorescence activated cell sorting.

596   Four populations were collected (top 5%, top 5-15%, lowest 5-15% and lowest 5%) based on

597   the cycK$_{eGFP}$ to mCherry mean fluorescent intensity (MFI) ratio. Sorted cells were harvested

598   by centrifugation and subjected to direct lysis as described above. The screen was analysed as

599   described previously by comparing stable populations (top 5% eGFP/mCherry expression) to

600   unstable populations (lowest 15% eGFP/mCherry expression). Hits enriched in cycK stable

601   population with FDR < 0.05 are labelled on the plot (Fig. 1g).

602

Pooled CRISPR screen data analysis

604   The data analysis pipeline comprised the following steps: (1) Each sample was normalised to

605   the total number of reads. (2) For each guide, the ratio of reads in the stable vs. unstable sorted

606   gate was calculated, and sgRNAs were ranked. (3) The ranks for each guide were summed for

607   all replicates. (3) The gene rank was determined as the median rank of the four guides targeting

608   it. (4) P-values were calculated by simulating a distribution with guide RNAs that had

609   randomly assigned ranks over 100 iterations. R scripts can be found in the Supplementary

610   Information.

611

DCAF arrayed screen

613   An arrayed DCAF library (targeting DCAFs substrate receptors, DCAF-like and control genes)

614   was constructed as described above with the appropriate oligos (Supplementary Oligo Table

615   1). K562$_{Cas9}$, P31FUJ$_{Cas9}$, THP1$_{Cas9}$ and MM1S$_{Cas9}$ were individually transduced and treated

616   with DMSO or 1 µM CR8 (K562$_{Cas9}$, P31FUJ$_{Cas9}$, THP1$_{Cas9}$) or 0.1 µM CR8 (MM1S$_{Cas9}$). The

617   analysis was performed as described above for validation of DDB1 resistance phenotype.

618

Protein purification

620   Human wild-type and mutant versions of DDB1 (Uniprot entry Q16531), CDK12 (Q9NYV4,

621   K965R) and CCNK (O75909) were subcloned into pAC-derived vectors[41] and recombinant

622   proteins were expressed as N-terminal His_6, His_6-Spy, StrepII or StrepII-Avi fusions in

623   *Trichoplusia ni* High Five insect cells using the baculovirus expression system (Invitrogen)[42].

624   Wild-type or mutant forms of full-length or beta-propeller B domain deletion (ΔBPB: aa 396-

625   705 deleted) constructs of His_6-DDB1 and StrepII-Avi-DDB1 were purified as previously

626   described for DDB1-DCAF complexes[9]. High Five insect cells co-expressing truncated

627   versions of wild-type or mutant His_6-CDK12 (aa 713-1052 or 713-1032) and His_6- or His_6-

628   Spy-tagged cycK (aa 1-267) were lysed by sonication in 50 mM Tris-HCl (pH 8.0), 500 mM

629   NaCl, 10% (v/v) glycerol, 10 mM $MgCl_2$, 10 mM imidazole, 0.25 mM tris(2-

630   carboxyethyl)phosphine (TCEP), 0.1% (v/v) Triton X-100, 1 mM

631   phenylmethylsulfonylfluoride (PMSF), and 1 x protease inhibitor cocktail (Sigma). Following

632   ultracentrifugation, the soluble fraction was passed over HIS-Select Ni^{2+} affinity resin (Sigma),

633   washed with 50 mM Tris-HCl (pH 8.0), 1 M NaCl, 10% (v/v) glycerol, 0.25 mM TCEP, 10

634   mM imidazole and eluted in 50 mM Tris-HCl (pH 8.0), 200 mM NaCl, 10% (v/v) glycerol,

635   0.25 mM TCEP, 250 mM imidazole. When necessary, affinity tags were removed by overnight

636   TEV protease treatment. In case of HIS-Select Ni^{2+} affinity purified CDK12-cycK that was not

637   subjected to TEV cleavage, the pH of the eluate was adjusted to 6.8 before ion exchange

638   chromatography. StrepII-tagged versions of CDK12-cycK were affinity purified using Strep-

639   Tactin Sepharose (IBA) omitting imidazole in lysis, wash and elution buffers, supplementing

640   the elution buffer with 2.5 mM desthiobiotin (IBA GmbH), and using 50 mM Tris-HCl (pH

641   6.8) throughout.

642   For ion exchange chromatography, affinity purified proteins were diluted in a 1:1 ratio with

643   buffer *A* (50 mM Tris-HCl (pH 6.8), 10 mM NaCl, 2.5% (v/v) glycerol, 0.25 mM TCEP) and

644   passed over an 8 mL Poros 50HQ column. The flow through was again diluted in a 1:1 ratio

645   with buffer *A* and passed over an 8 mL Poros 50HS column. Bound proteins were eluted by a

646   linear salt gradient mixing buffer *A* and buffer *B* (50 mM Tris-HCl (pH 6.8), 1 M NaCl, 2.5%

647   (v/v) glycerol, 0.25 mM TCEP) over 15 column volumes to a final ratio of 80% buffer *B*. Poros

648   50HS peak fractions containing the CDK12-cycK complex were concentrated and subjected to

649   size exclusion chromatography in 50 mM HEPES (pH 7.4), 200 mM NaCl, 2.5% (v/v) glycerol

650   and 0.25 mM TCEP. The concentrated proteins were flash frozen in liquid nitrogen and stored

651   at -80°C.

652

653   **Co-immunoprecipitation assay**

654   The purified His_6-CDK12/StrepII-cycK complex was mixed with equimolar concentrations of

655   full-length His_6-DDB1 or TEV-cleaved DDB1^{ΔBPB} (5 μM) in the presence 5 μM *R*-CR8 or

656   DMSO in IP buffer (50 mM HEPES (pH 7.4), 200 mM NaCl, 0.25 mM TCEP, 0.05% (v/v)

657   Tween-20) containing 1 mg/mL bovine serum albumin. The solution was added to Strep-Tactin

658   MacroPrep beads (IBA GmbH) preequilibrated in IP buffer and incubated for 1 hour at 4°C on

659   an end-over-end shaker. The beads were extensively washed with IP buffer, and the bound

660   protein was eluted with IP buffer containing 2.5 mM desthiobiotin for 1 hour at 4°C on an end-

661   over-end shaker. Eluted proteins were separated by SDS-PAGE stained with Coomassie

662   Brilliant Blue.

663

Crystallization and data collection

665   The protein solution for crystallization contained 70 μM TEV-cleaved DDB1$^{\Delta BPB}$, 80 μM R-

666   CR8 and 80 μM TEV-cleaved CDK12-cycK in 50 mM HEPES (pH 7.4), 200 mM NaCl, 0.25

667   mM TCEP. Crystals were grown by vapour diffusion in drops containing 1 μL

668   DDB1$^{\Delta BPB}$-R-CR8-CDK12$^{713-1052}$-cycK$^{1-267}$ complex solution mixed with 1 μL of reservoir

669   solution containing 0.9 M ammonium citrate tribasic (pH 7.0) in two-well format sitting drop

670   crystallization plates (Swissci). Plates were incubated at 19°C and crystals appeared 5-13 days

671   after setup. Crystals were flash cooled in liquid nitrogen in reservoir solution supplemented

672   with 25% (v/v) glycerol as a cryoprotectant prior to data collection. Diffraction data were

673   collected at the Swiss Light Source (beamline PXI) with an Eiger 16M detector (Dectris) at a

674   wavelength of 1 Å and a crystal cooled to 100 K. Data were processed with *DIALS*, scaled with

675   *AIMLESS* supported by other programs of the CCP4 suite[43], and converted to structure factor

676   amplitudes with *STARANISO*[44], applying a locally weighted $CC_{1/2} = 0.3$ resolution cutoff.

677

Structure determination and model building

679   The DDB1$^{\Delta BPB}$–R-CR8-CDK12$^{713-1052}$-cycK$^{1-267}$ complex formed crystals belonging space

680   group $P3_121$, with three complexes in the crystallographic asymmetric unit (ASU). Their

681   structure was determined using molecular replacement (MR) in *PHASER*[45] with a search model

682   derived from PDB entry 6H0F for DDB1$^{\Delta BPB}$, and PDB entry 4NST for CDK12-cycK. The

683   initial model was improved by iterative cycles of building with *COOT*[46], and refinement using

684   *phenix.refine*[47] or *autoBUSTER*[48], with ligand restraints generated using *eLBOW* through

685   *phenix.ready_set*[49]. The final model was produced by refinement with *autoBUSTER*. Analysis

686   with *MOLPROBITY*[50]. indicates that 93.9% of the residues in final model are in favourable

687   regions of the Ramachandran plot, with 0.6% outliers. Data processing and refinement statistics

688   are in Extended Data Table 1. Interface analysis was performed using PISA[51].

689

Biotinylation of DDB1

Purified full-length StrepII-Avi-DDB1 was biotinylated *in vitro* at a concentration of 8 μM by incubation with final concentrations of 2.5 μM BirA enzyme and 0.2 mM D-biotin in 50 mM HEPES (pH 7.4), 200 mM NaCl, 10 mM $MgCl_2$, 0.25 mM TCEP and 20 mM ATP. The reaction was incubated for 1 hour at room temperature and stored at 4°C for 14-16 hours. Biotinylated DDB1 ($_{biotin}$DDB1) was purified by gel filtration chromatography and stored at -80°C (~20 μM).

Time-resolved fluorescence resonance energy transfer (TR-FRET)

Increasing concentrations of Alexa488-SpyCatcher-labelled[27] His_6-Spy-cycK/His_6-CDK12 ($_{Alexa488}$cycK-CDK12) were added to a mixture of biotinylated DDB1 ($_{biotin}$DDB1) at 50 nM, terbium-coupled streptavidin at 4 nM (Invitrogen) and kinase inhibitors at 10 μM (final concentrations) in 384-well microplates (Greiner, 784076) in a buffer containing 50 mM Tris (pH 7.5), 150 mM NaCl, 0.1% pluronic acid and 0.5% DMSO (see also figure legends). CR8 titrations were carried out by adding increasing concentrations CR8 (0-25 μM) into premixed 500 μM $_{Alexa488}$cycK-CDK12, 50 nM $_{biotin}$DDB1, and 4 nM terbium-coupled streptavidin. Before TR-FRET measurements, reactions were incubated for 15 minutes at room temperature. After excitation of terbium (Tb) fluorescence at 337 nm, emissions at 490 nm (Tb) and 520 nm (Alexa488) were measured with a 70 μs delay to reduce background fluorescence and the reactions were followed by recording 60 data points of each well over 1 hours using a PHERAstar FS microplate reader (BMG Labtech). The TR-FRET signal of each data point was extracted by calculating the 520:490 nm ratio. Data were analysed with *Prism* 7 (GraphPad) assuming equimolar binding of $_{biotin}$DDB1 to $_{Alexa488}$cycK-CDK12 using the equations described previously[8].

Counter titrations with unlabelled proteins were carried out by mixing 500 μM $_{Alexa488}$cycK-CDK12 with 50 nM $_{biotin}$DDB1 in the presence of 4 nM terbium-coupled streptavidin and 1 μM compound for DDB1 titrations or 12.5 μM compound for CDK12 titrations. After incubation for 15 minutes at room temperature, increasing amounts of unlabelled cycK-CDK12 or DDB1 (0-10 μM) were added to the preassembled $_{Alexa488}$cycK-CDK12/$_{biotin}$DDB1 complexes in a 1:1 volume ratio and incubated for 15 minutes at room temperature. TR-FRET data were acquired as described above. The 520/490 nm ratios were plotted to calculate the half maximal inhibitory concentrations (IC_{50}) assuming a single binding site using *Prism* 7 (GraphPad). IC_{50} values

723   were converted to the respective K_i values as described previously[52]. Three technical replicates

724   were carried out per experiment.

725

726   **DDB1-CUL4-RBX1 reconstitution and *in vitro* CUL4 neddylation**

727   *In vitro* CRL4 reconstitution and CUL4 neddylation were performed as described[8]. His_6-

728   CUL4A/His_6-RBX1 at 3.5 µM was incubated with His_6-DDB1 at 3 µM in a reaction mixture

729   containing 3.8 µM NEDD8, 50 nM NAE1/UBA3 (E1), 30 nM UBC12 (E2), 1 mM ATP, 50

730   mM Tris (pH 7.5), 100 mM NaCl, 2.5 mM $MgCl_2$, 0.5 mM DTT and 5% (v/v) glycerol for 1.5

731   hours at room temperature. Neddylated and gel filtration-purified DDB1-CUL4-RBX1

732   ($_{N8}$DDB1-CUL4-RBX1) was concentrated to 7.6 µM, flash frozen and stored at -80°C.

733

734   **In-vitro ubiquitination assays**

735   *In vitro* ubiquitination was performed by mixing $_{N8}$DDB1-CUL4-RBX1 at 70 nM with a

736   reaction mixture containing kinase inhibitors at 2 µM, CDK12-cycK at 500 nM, E1 (UBA1,

737   BostonBiochem) at 50 nM, E2 (UBCH5a, BostonBiochem) at 1 µM, and ubiquitin at 20 µM.

738   Reactions were carried out in 50 mM Tris (pH 7.5), 150 mM NaCl, 5 mM $MgCl_2$, 0.2 mM

739    $CaCl_2$, 1 mM ATP, 0.1% Triton X-100 and 0.1 mg/mL BSA, incubated for 0-30 minutes at

740   30°C and analysed by western blot using anti-cycK and anti-rabbit IgG antibodies. Blots were

741   scanned on an Amersham 600 CCD-based imaging system (GE Life Sciences).

742

743   **Isothermal titration calorimetry (ITC)**

744   ITC experiments were performed at 25°C on a VP-ITC isothermal titration calorimeter

745   (Microcal Inc.). Purified and TEV-cleaved CDK12-cycK and DDB1$^{\Delta BPB}$ were exhaustively

746   dialysed in 50 mM HEPES (pH 7.4), 150 mM NaCl, 0.25 mM TCEP, 0.5% DMSO and loaded

747   into the sample cell at a final concentration of 10-50 µM. Kinase inhibitors (CR8 or roscovitine)

748   were diluted from a 100 mM DMSO stock solution to 100-500 µM in buffer containing 50 mM

749   HEPES (pH 7.4), 150 mM NaCl, 0.25 mM TCEP. The final DMSO concentration was 0.5%.

750   Titrations with 100-500 µM compound were performed typically through about 30 injections

751   of 6-10 µL at 210 second intervals from a 300 µL syringe rotating at 300 rpm. An initial

752   injection of the ligand (4 µL) was made and discarded during data analysis. For probing DDB1-

753   CDK12-cycK complex formation, DDB1$^{\Delta BPB}$ (100 µM, in the syringe) was titrated into the cell

754   containing CDK12-cycK (10 µM) or CDK12-cycK (10 µM) pre-incubated with CR8 (30 µM).

755   The heat change accompanying the titration was recorded as differential power by the

756   instrument and determined by integration of the peak obtained. Titrations of ligand to buffer

only and buffer into protein were performed to allow baseline corrections. The heat change was fitted using nonlinear least-squares minimization to obtain the dissociation constants, K_d, the enthalpy of binding, ΔH, and the stoichiometry, n. Between one and three replicates were performed per titration.

Bioluminescence Resonance Energy Transfer (BRET) analyses

Bioluminescence resonance energy transfer (BRET) experiments were using a NanoBRET PPI starter kit (Promega N1821) according to the manufacturer's instructions and as previously described[53].

Drug sensitivity assays

HEK293T$_{Cas9}$ cells were resuspended at 0.15×10^6 per mL and plated on a 384 well plate with 50 µl per well and MLN4924, MLN7243 or MG132 with or without CR8 serially diluted with D300e Digital Dispenser (Tecan Inc.).

HEK293T$_{Cas9}$ cells (0.625×10^6 cells/6 well plate format) were seeded the day before transfection. The following day, 2.5 ug of pRSF91-GFP or pRSF91-CRBN[6] plasmid DNA was mixed with 250 µl OptiMem and 7.5 µl TransIT-LT1 (Mirus Bio) according to manufacture protocol. 48 hours post transfection cells were resuspended at 0.15×10^6 cells /mL and plated on a 384 well plate with 50 µl per well.

HEK293T$_{Cas9}$ cells were transduced with sgRNAs targeting either DDB1 or Luciferase in pXPR003 backbone (GPP) (Supplementary Oligo Table 1). After nine days of puromycin selection, cells were re-plated into a 96-well format with 2×10^4 cells per well and CR8 and Roscovitine were serially diluted with D300e Digital Dispenser (Tecan Inc.).

After 3 days of drug exposure, cell viability was assessed using the CellTiter-Glo luminescent assay (Promega, #G7572) on an EnVision Multilabel Plate Reader (Perkin Elmer). Cell viabilities were calculated relative to DMSO controls.

CycK stability reporter analysis with CRBN overexpression

HEK293T$_{Cas9}$ cells expressing the cycK$_{eGFP}$ degradation reporter were transiently transfected with pLX307-Luc or pLX307-CRBN (for flow experiment) as described above and 48 hours post infection treated with CR8 for 2 hours and analysed by flow cytometry.

791

Data Availability
Data necessary to reproduce statistical analysis are included in Supplementary Materials.
794

Code Availability
Code necessary to reproduce statistical analysis is included in Supplementary Materials.
797

798

Supplementary References

36. Sievers, Q. L., Gasser, J. A., Cowley, G. S., Fischer, E. S. & Ebert, B. L. Genome-wide screen identifies cullin-RING ligase machinery required for lenalidomide-dependent CRL4CRBN activity. *Blood* **132**, 1293–1303 (2018).

37. Doench, J. G. *et al.* Optimized sgRNA design to maximize activity and minimize off-target effects of CRISPR-Cas9. *Nat. Biotechnol.* **34**, 184–191 (2016).

38. Sanjana, N. E., Shalem, O. & Zhang, F. Improved vectors and genome-wide libraries for CRISPR screening. *Nat. Methods* **11**, 783–784 (2014).

39. Donovan, K. A. *et al.* Thalidomide promotes degradation of SALL4, a transcription factor implicated in Duane radial ray syndrome. *Elife* **7**, (2018).

40. Benjamini, Y. & Hochberg, Y. Controlling the False Discovery Rate: A Practical and Powerful Approach to Multiple Testing. *J. R. Stat. Soc. Ser. B* **57**, 289–300 (1995).

41. Abdulrahman, W. *et al.* A set of baculovirus transfer vectors for screening of affinity tags and parallel expression strategies. *Anal. Biochem.* **385**, 383–5 (2009).

42. Li, T., Pavletich, N. P., Schulman, B. A. & Zheng, N. High-level expression and purification of recombinant SCF ubiquitin ligases. *Methods in Enzymology* vol. 398 125–142 (2005).

43. Winn, M. D. *et al.* Overview of the CCP4 suite and current developments. *Acta Crystallogr. D. Biol. Crystallogr.* **67**, 235–42 (2011).

44. Tickle, I.J., Flensburg, C., Keller, P., Paciorek, W., Sharff, A., Vonrhein, C., Bricogne, G. STARANISO. (2018).

45. McCoy, A. J. *et al.* Phaser crystallographic software. *J. Appl. Crystallogr.* **40**, 658–674 (2007).

46. Emsley, P., Lohkamp, B., Scott, W. G. & Cowtan, K. Features and development of Coot. *Acta Crystallogr. D. Biol. Crystallogr.* **66**, 486–501 (2010).

47. Afonine, P. V *et al.* Towards automated crystallographic structure refinement with phenix.refine. *Acta Crystallogr. D. Biol. Crystallogr.* **68**, 352–67 (2012).

48. Bricogne, G. B. E. BUSTER. (2011).

49. Moriarty, N. W., Grosse-Kunstleve, R. W. & Adams, P. D. electronic Ligand Builder and Optimization Workbench (eLBOW): a tool for ligand coordinate and restraint generation. *Acta Crystallogr. D. Biol. Crystallogr.* **65**, 1074–80 (2009).

50. Chen, V. B. *et al.* MolProbity: All-atom structure validation for macromolecular crystallography. *Acta Crystallogr. Sect. D Biol. Crystallogr.* **66**, 12–21 (2010).

51. Krissinel, E. & Henrick, K. Inference of Macromolecular Assemblies from Crystalline State. *J. Mol. Biol.* **372**, 774–797 (2007).

52. Cer, R. Z., Mudunuri, U., Stephens, R. & Lebeda, F. J. IC50-to-Ki: a web-based tool for converting IC50 to Ki values for inhibitors of enzyme activity and ligand binding. *Nucleic Acids Res.* **37**, 441–5 (2009).

53. Sperling, A. S. *et al.* Patterns of substrate affinity, competition, and degradation kinetics underlie biological activity of thalidomide analogs. *Blood* **134**, 160–170 (2019).

Author contributions

M.S. performed functional genomics studies with the help of J.K., R.S.S., E.C.F.; Z.K., G.P. designed and carried out structural, biochemical and biophysical studies with the help of D.S.; M.S., Y.D.L., M.M., Q.L.S. designed and performed validation cell experiments with the help of A.S.S., J.A.G., M.J.; K.A.D. performed the mass spectrometry experiments; M.S., L.R.W. and S.M.C. performed bioinformatic PRISM analysis; R.B., G.P. performed structure refinement with the help of Z.K.; D.G., C.S., S.F., T.R.G, E.S.F, N.H.T., B.L.E supervised the project, Z.K., G.P., M.S, B.L.E., N.H.T wrote the manuscript with input from all authors.

Conflict-of-interest disclosure

B.L.E. has received research funding from Celgene and Deerfield. He has received consulting fees from GRAIL, and he serves on the scientific advisory boards for and holds equity in Skyhawk Therapeutics and Exo Therapeutics. E.S.F. is a founder and/or member of the scientific advisory board (SAB), and equity holder of C4 Therapeutics and Civetta Therapeutics and a consultant to Novartis, AbbVie and Pfizer. N.H.T receives funding from the Novartis Research Foundation and is an SAB member of Monte Rosa Therapeutics. The Fischer lab receives or has received research funding from Novartis, Deerfield and Astellas.

896 **Additional Information**
897 Correspondence and requests for materials should be addressed to N.H.T. and B.L.E.
898
899
900
901

a
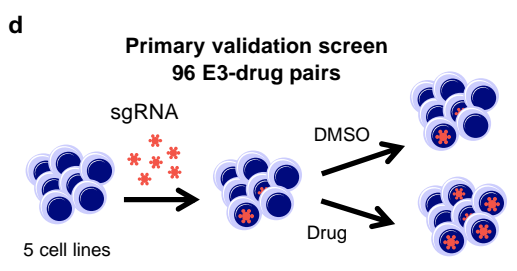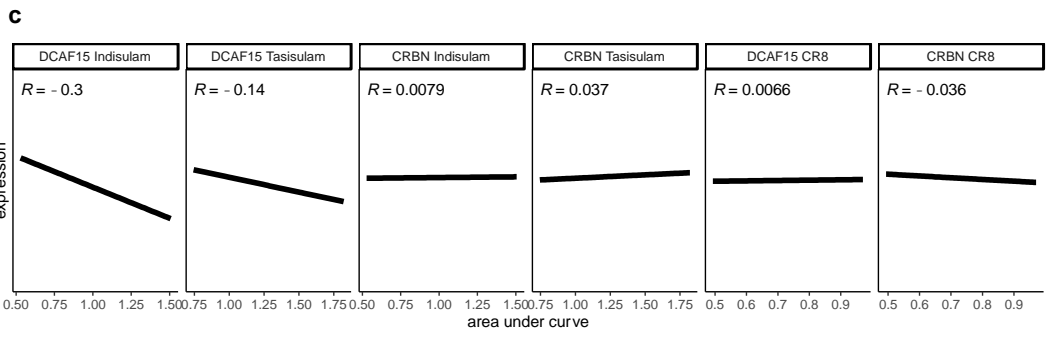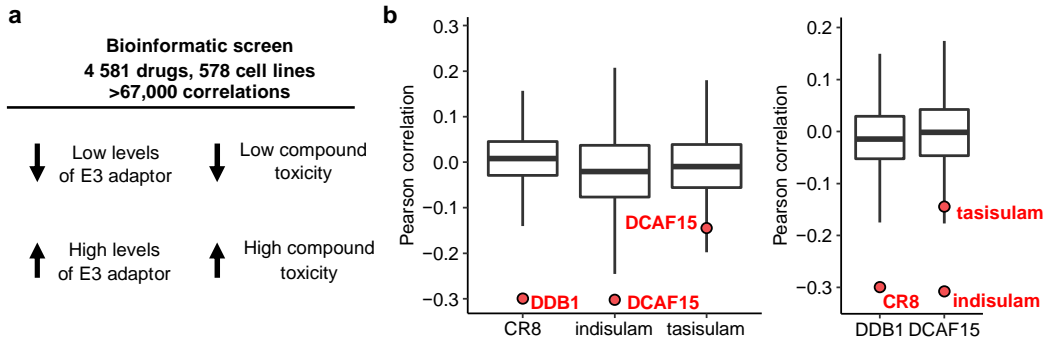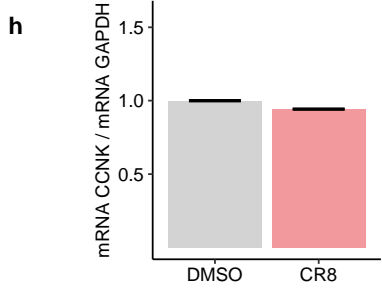
Bioinformatic screen
4 581 drugs, 578 cell lines
>67,000 correlations

| ↓ Low levels of E3 adaptor | ↓ Low compound toxicity |
| ↑ High levels of E3 adaptor | ↑ High compound toxicity |

b

c

DCAF15 Indisulam $R = -0.3$ DCAF15 Tasisulam $R = -0.14$ CRBN Indisulam $R = 0.0079$ CRBN Tasisulam $R = 0.037$ DCAF15 CR8 $R = 0.0066$ CRBN CR8 $R = -0.036$

d

Primary validation screen
96 E3-drug pairs

sgRNA

DMSO

Drug

5 cell lines

e

Ranking	Gene	Drug
1	DCAF15	indisulam
2	DDB1	CR8
3	DCAF15	tasisulam

f

Decreased upon CR8   Whole Proteome

g

h
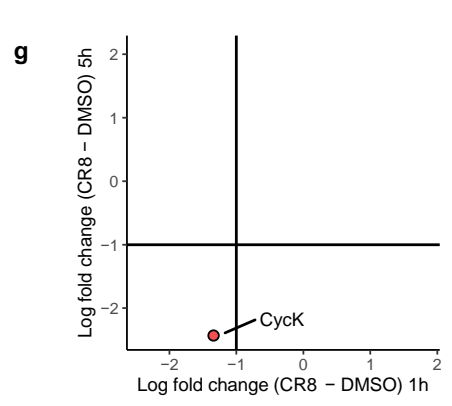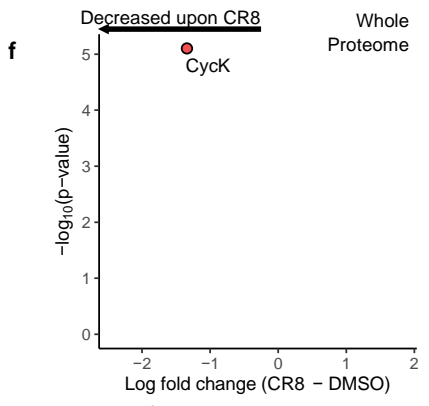
902
903

904 **Extended Data Figure 1 | CR8-induced degradation of cycK correlates with DDB1 expression. a**,
905 Schematic of bioinformatic screen for identification of novel correlations between drug toxicity and E3
906 ligase mRNA expression. **b**, Box-and-whisker plot representing expression–sensitivity correlations for
907 CR8, indisulam and tasisulam sensitivity as well as DDB1 and DCAF15 expression. **c**, Correlation of
908 indisulam and tasisulam toxicity with mRNA expression of DCAF15. Selected negative correlations
909 are included for comparison. **d**, Schematic of flow-based primary validation screen. **e**, Top three hits
910 from the primary validation screen in 5 cell lines, performed according to schematic outline on Extended
911 Data Figure 1d. **f**, Molt-4 cells were exposed to 1 µM CR8 or DMSO for 1 hour followed by whole
912 proteome quantification using tandem mass tag mass spectrometry (mean log2 fold change, p value
913 calculated by a moderated t-test), n=3 (DMSO), n=1 (CR8). **g**, The log2 fold changes in whole proteome
914 quantification after 1 and 5 hours of exposure to CR8 are plotted against each other. **h**, HEK293T$_{Cas9}$
915 cells were treated with 1 µM CR8 or DMSO for 2 hours and CCNK mRNA levels were measured by
916 quantitative PCR. Bars represent the mean ± s.d. (n=3).
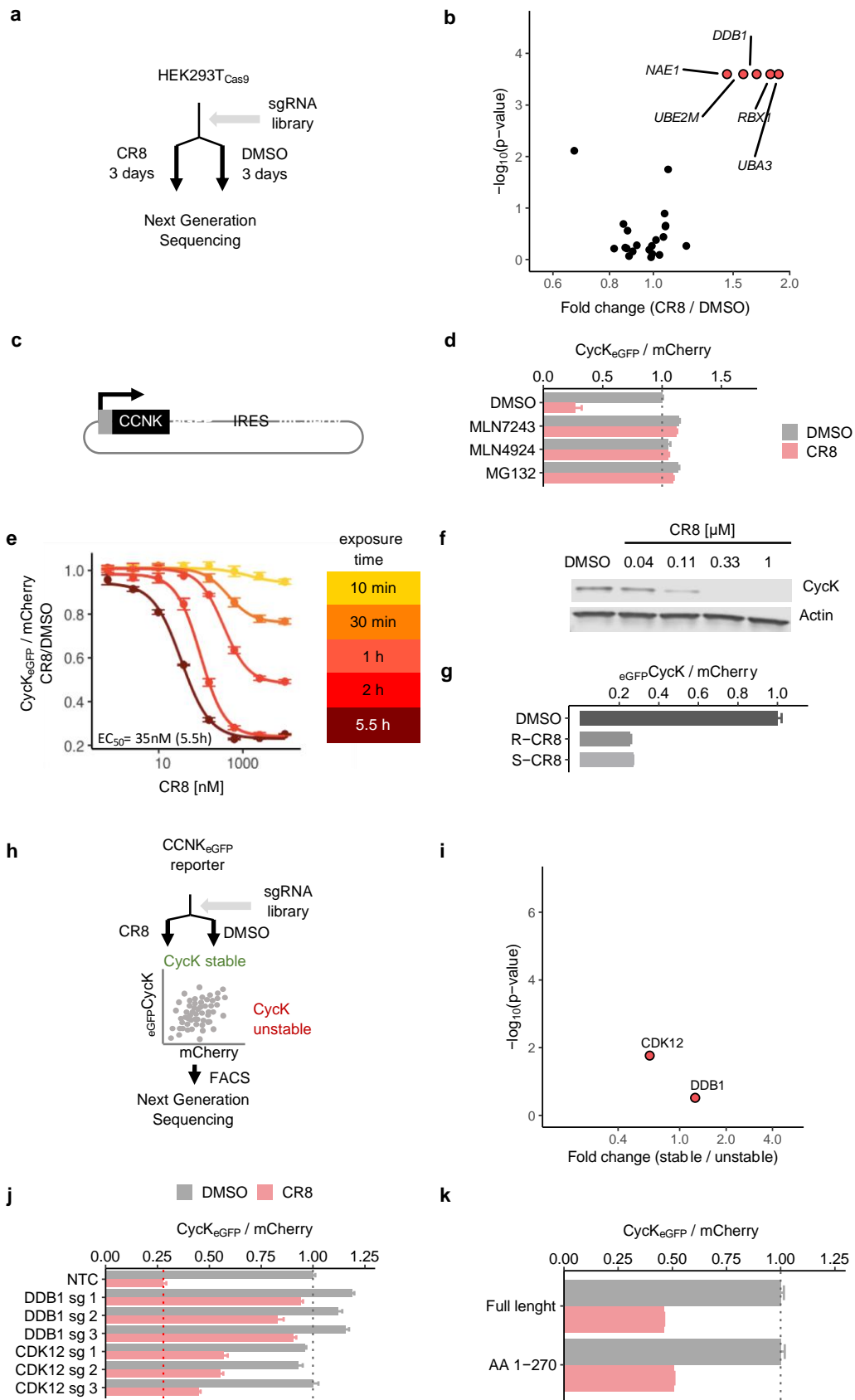
917
918 **Extended Data Figure 2 | CDK12 is required for CR8-induced cycK degradation. a,** Schematic of
919 the genome-wide CRISPR-Cas9 resistance screen. **b,** Median fold change of read counts (CR8/DMSO
920 treatment) and corresponding p values (empirical rank-sum test-statistic) for sgRNAs targeting 713 E1,

921   E2, E3, DUB and control genes (BISON library) conferring resistance to CR8 treatment. DCAF
922   substrate receptors are labelled with black dots (n=3) **c**, Schematic of the cycK (*CCNK*) stability
923   reporter. eGFP, enhanced green fluorescent protein, IRES, internal ribosome entry site. **d**, CycK$_{eGFP}$
924   HEK293T$_{Cas9}$ cells were treated as described in Fig. 1D and analysed by flow cytometry. Bars represent
925   the mean ± s.d. (n=3). **e**, CycK$_{eGFP}$ HEK293T$_{Cas9}$ cells were exposed to various concentration of CR8
926   and analysed by flow cytometry. Data represent mean ± s.d. Lines represent standard four-parameter
927   log-logistic curves (n=3). **f**, HEK293T$_{Cas9}$ cells were treated with indicated concentration of CR8 for 2
928   hours and lysates were immunoblotted for the indicated targets. **g**, CycK$_{eGFP}$ HEK293T$_{Cas9}$ cells were
929   treated with 1 µM of the indicated compound for 2 hours and analysed by flow cytometry. Data
930   represent mean ± s.d. Line represents standard four parameter log-logistic curves (n=3). **h**, Schematic
931   of the genome-wide CRISPR-Cas9 reporter screen. **i**, Median fold change of read counts (cycK
932   stable/unstable) and corresponding p values (empirical rank-sum test-statistic) in the absence of CR8
933   for sgRNAs targeting 19,112 human genes in HEK293T$_{Cas9}$ cells (n=2). **j**, CycK$_{eGFP}$ HEK293T$_{Cas9}$ cells
934   were transfected with blue fluorescent protein (BFP) and sgRNAs, treated with DMSO or 1 µM CR8
935   and analysed by flow cytometry. Bars represent the mean ± s.d. (n=3). **k**, CycK$_{eGFP}$^{Full Lenght} HEK293T$_{Cas9}$
936   or CycK$_{eGFP}$^{AA1-270} HEK293T$_{Cas9}$ were treated with DMSO or 1 µM CR8 and analysed by flow
937   cytometry. Bars represent the mean ± s.d. (n=3).

938
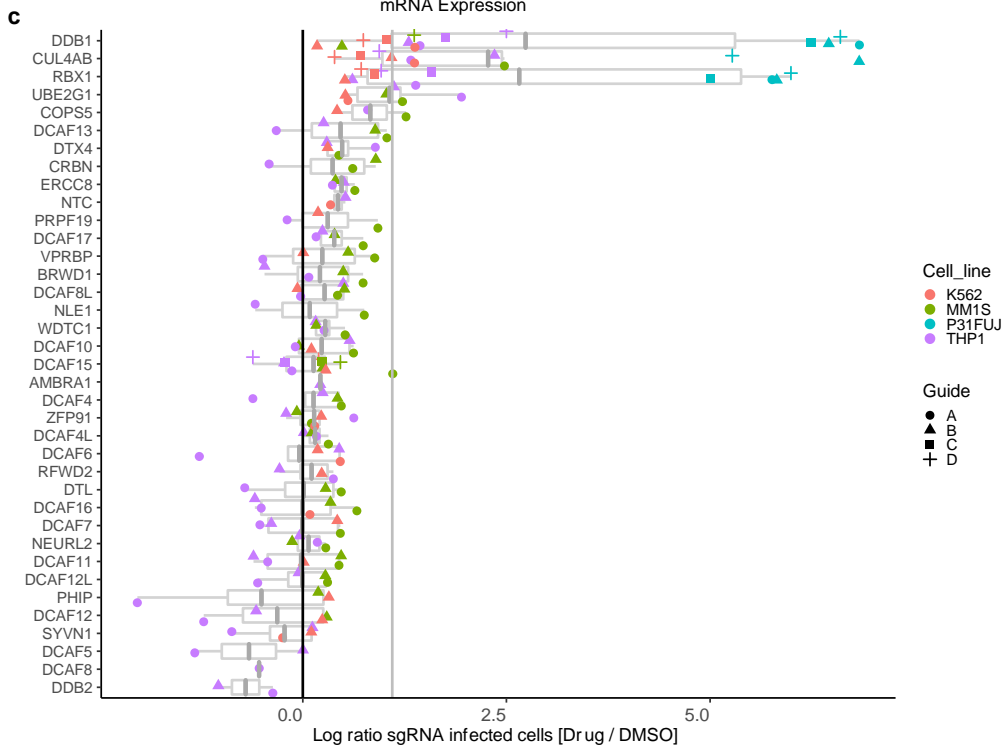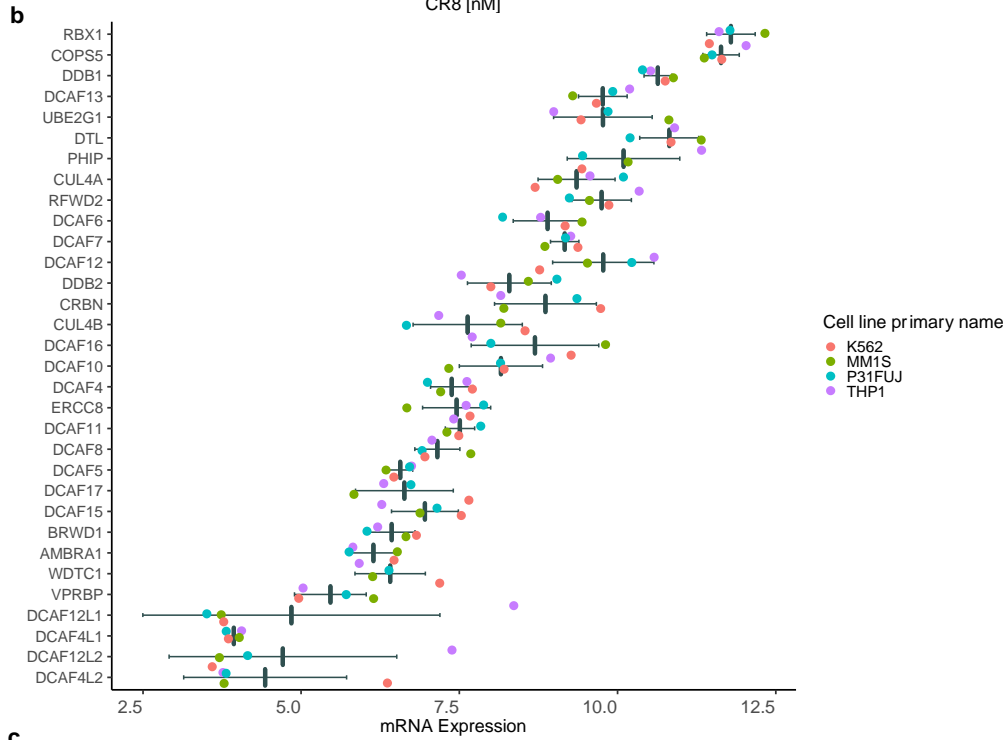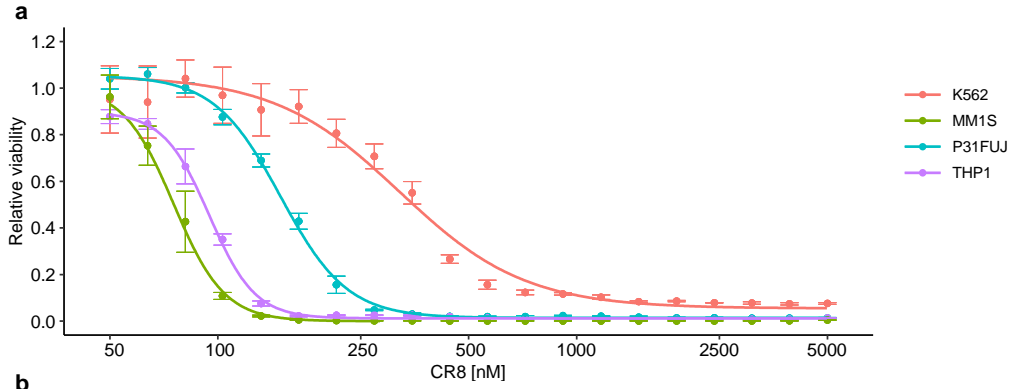
939 **Extended Data Figure 3 | CR8-induced cycK degradation is not dependent on any DCAF**
940 **substrate receptor. a**, K562$_{Cas9}$, P31FUJ$_{Cas9}$, THP1$_{Cas9}$ and MM1S$_{Cas9}$ cells were exposed to the
941 indicated concentrations of CR8 for 3 days. Data represent mean ± s.d. Lines represent standard four-
942 parameter log-logistic curves. **b**, mRNA expression levels for all genes included in DCAF library. **c**,
943 K562$_{Cas9}$, P31FUJ$_{Cas9}$, THP1$_{Cas9}$ and MM1S$_{Cas9}$ were individually transduced with arrayed DCAF library
944 and treated with 1 μM CR8 (K562$_{Cas9}$, P31FUJ$_{Cas9}$, THP1$_{Cas9}$) or 0.1 μM CR8 (MM1S$_{Cas9}$) and ratio of
945 transduced to untransduced cells was determined using flow cytometry (n=1).
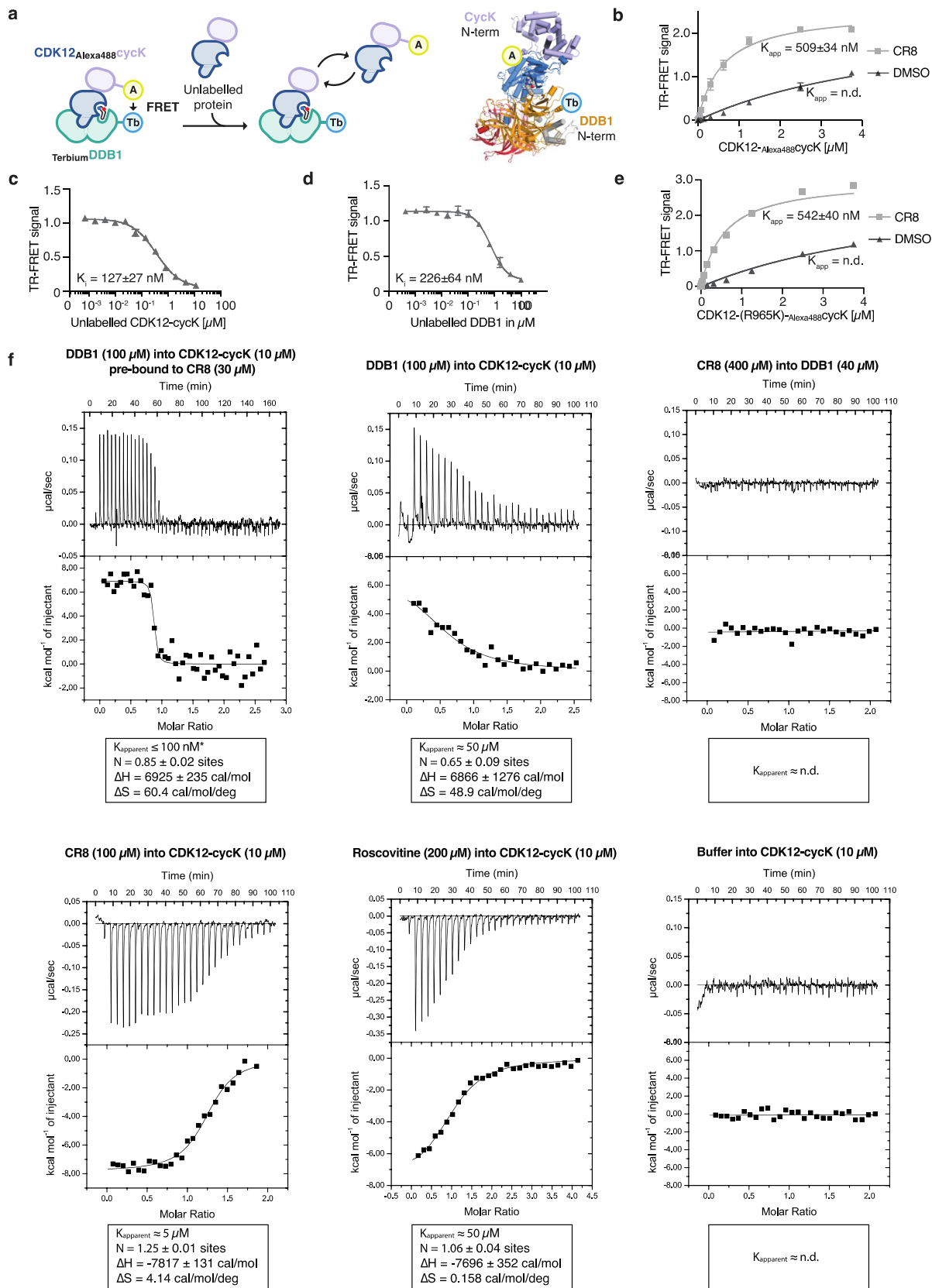
948 **Extended Data Figure 4 | Characterization of the CR8-induced DDB1-CDK12-cycK interaction.**
949 **a**, Schematic of the TR-FRET setup. Positions of the FRET donor (Terbium-streptavidin (T)) and
950 acceptor (Alexa488-labeled SpyCatcher (A)) are indicated in the structural model of DDB1$^{\Delta BPB}$CDK12-
951 CR8-cycK on the right. **b**, TR-FRET titration of CDK12-$_{Alexa488}$cycK (0-3.75 µM) to 50 nM $_{Terbium}$DDB1

952   and 5 µM CR8 or DMSO. Data represent the mean ± s.d. (n=3). **c**, TR-FRET counter titration of
953   unlabelled wild-type CDK12-cycK to 50 nM $_{Terbium}$DDB1, 500 nM CDK12-$_{Alexa488}$cycK and 12.5 µM
954   CR8. Data represent the mean ± s.d. (n = 3). **d**, TR-FRET counter titration of unlabelled wild-type
955   DDB1 to 50 nM $_{Terbium}$DDB1, 500 nM CDK12-$_{Alexa488}$cycK and 1 µM CR8. Data represent the mean ±
956   s.d. (n=3). **e**, TR-FRET titration of CDK12(R965K)-$_{Alexa488}$cycK (wild-type sequence of canonical
957   isoform of CDK12; 0-3.75 µM) to 50 nM $_{Terbium}$DDB1 and 5 µM CR8 or DMSO. Data represent the
958   mean ± s.d. (n=3). The CDK12 K965R variant (residue distal from the interface with DDB1 and cycK),
959   which was used throughout our *in vitro* studies (see methods), shows a binding affinity indistinguishable
960   from that of wild-type CDK12. **f**, Isothermal titration calorimetry (ITC) experiments (n =1-3, additional
961   replicates provided in Supplementary ITC Data). Specifications of the individual experiments are given
962   in the panel. Asterisk marking the approximate $K_{apparent}$ value in the first panel denotes that the binding
963   affinity was too high to allow confident fitting of the binding curve.
964
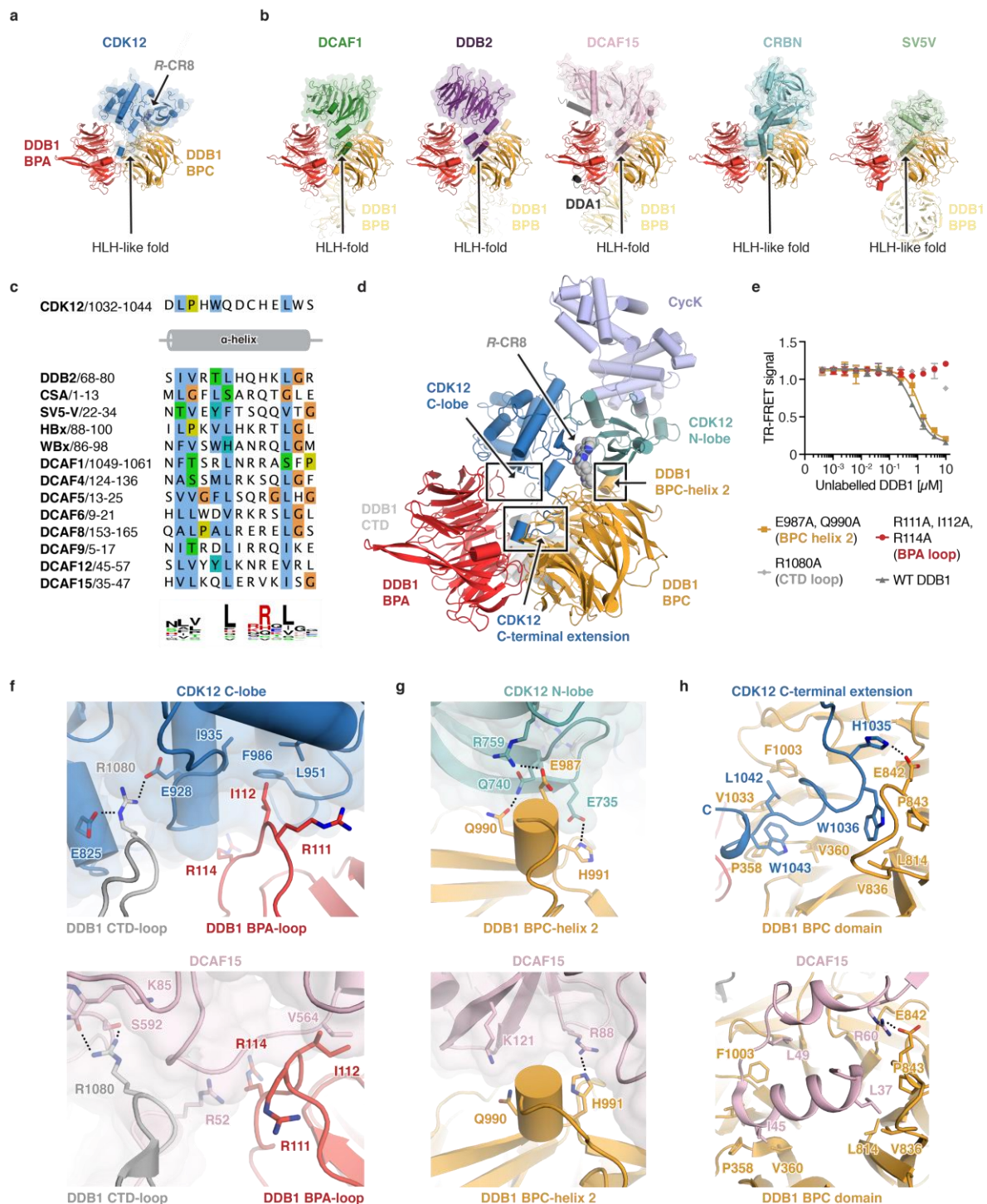
965
966 **Extended Data Figure 5 | CDK12 contacts sites on DDB1 otherwise implicated in DCAF binding.**
967 **a**, Structure of the CDK12-*R*-CR8-DDB1$^{\Delta BPB}$ complex. The CDK12 C-terminal domain binds a cleft
968 between the BPA and BPC domains of DDB1 (arrow) and adopts an helix-loop-helix (HLH)-like fold.
969 **b**, Diverse DDB1-CUL4 associated factors (DCAFs) bind DDB1 BPA and BPC domains through HLH-
970 or HLH-like folds. **c**, Protein sequence alignment of identically positioned HLH-domain helices from
971 different DCAFs. **d**, Protein-protein interaction hotspots highlighted in the structure of the
972 DDB1$^{\Delta BPB}$CDK12-CR8-cycK complex. **e**, TR-FRET counter titration of unlabelled wild-type or mutant
973 DDB1 (0-10 μM) into pre-assembled $_{Terbium}$DDB1-CR8-CDK12-$_{Alexa488}$cycK complex. Data represent
974 the mean ± s.d. (n = 3). **f**, Close-up of the interface between the CDK12 C-lobe and DDB1 loop residues
975 provided by the BPA and CTD domains (top). These DDB1 residues also form contacts with DCAF15
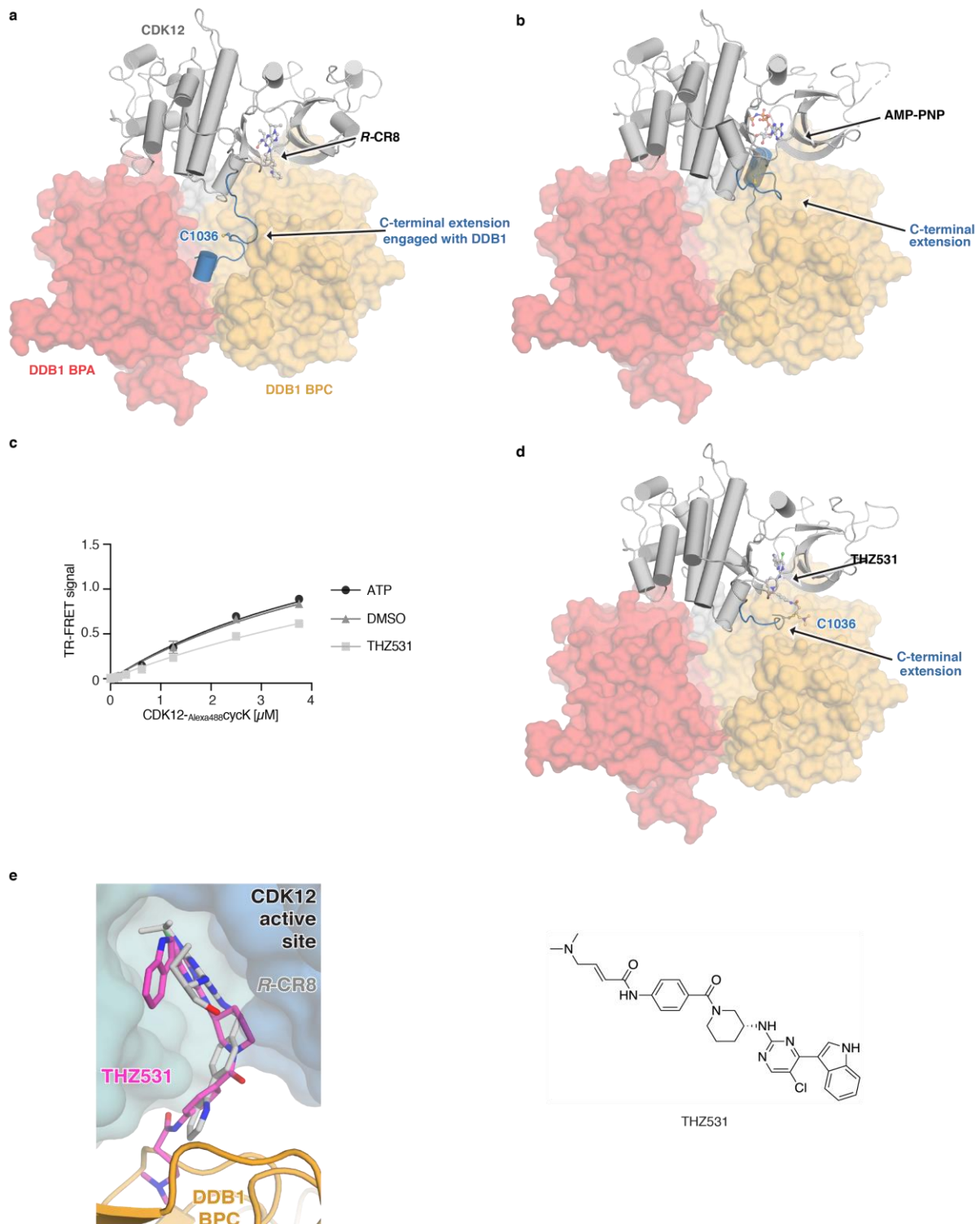976 (bottom). **g**, Close-up of the interface between the CDK12 N-lobe and DDB1 BPC-helix 2 (top). Similar

41

977 DDB1 residues contact DCAF15 (bottom). **h**, Close-up of the interface between the CDK12 C-terminal
978 extension and BPC domain of DDB1 (top). Similar DDB1 residues interact with DCAF15 (bottom).

979
Extended Data Figure 6 | C-terminal extension of CDK12 adopts different conformations. a,
Structure of the CDK12-CR8-DDB1$^{\Delta BPB}$ complex highlighting position and conformation of the
CDK12 C-terminal extension binding the cleft between the BPA and BPC domains of DDB1. **b**,
Structure of CDK12 bound to AMP-PNP (PDB entry 4CXA) superimposed onto CDK12 in the
CDK12-CR8-DDB1$^{\Delta BPB}$ complex. In the AMP-PNP-bound form of CDK12, the C-terminal extension
is in a conformation that allows contacts with the nucleotide analogue. This conformation of the CDK12
C-terminal extension is incompatible with DDB1 binding. **c**, TR-FRET titration of CDK12-$_{Alexa488}$cycK
(0-3.75 µM) to 50 nM $_{Terbium}$DDB1 in the presence of 5 µM THZ531, ATP or DMSO. Data represent
the mean ± s.d. (n=3). **d**, Structure of CDK12 bound to THZ531 (PDB entry 5ACB) superimposed onto

43

989 CDK12 in the CDK12-CR8-DDB1$^{\Delta BPB}$ complex. This conformation of the CDK12 C-terminal
990 extension is incompatible with DDB1 binding. **e**, THZ531 binding pose in the active site of CDK12
991 (PDB entry 5ACB) superimposed on the CR8-bound CDK12 in the DDB1$^{\Delta BPB}$CR8-CDK12-cycK
992 complex.

**a**, Protein sequence alignment of CDK12 (727-1052) and CDK13 (705-1030).
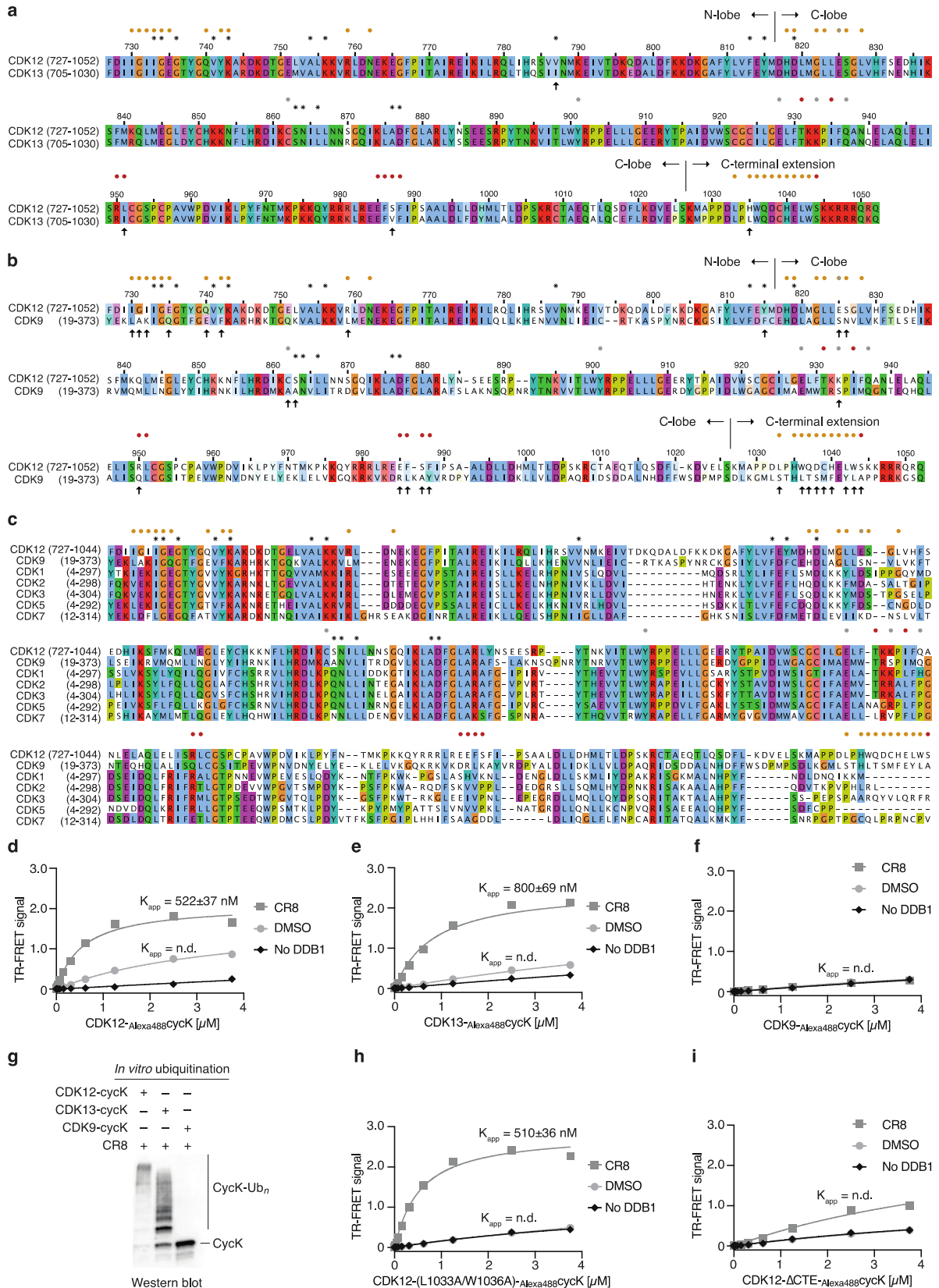
993
994
995
996
997
998
45

Extended Data Figure 7 | Interface differences between CDK12 and other CDKs highlight residues involved in CR8-mediated recruitment to DDB1.
**a**, Protein sequence alignment of CDK12 (727-1052) and CDK13 (705-1030). In this and later panels residues that contact CR8 are marked by an asterisk, those that contact DDB1 by dots that are coloured according to the domain organisation of DDB1 (see Fig. 2). Arrows mark differences at the DDB1-

999 CR8-CDK interface. **b**, Protein sequence alignment of CDK12 (727-1052) and CDK9 (19-373). **c**,
1000 Protein sequence alignment of CDK12 (727-1052), CDK9 (19-373), CDK1 (4-297), CDK2 (4-298),
1001 CDK3 (4-304), CDK5 (4-292), CDK7 (12-314). **d**, TR-FRET titration of CDK12-$_{Alexa488}$cycK (0-3.75
1002 µM) to 50 nM $_{Terbium}$DDB1 and 5 µM CR8 or DMSO. The no-DDB1 control in this and subsequent
1003 panels contained streptavidin-terbium and shows concentration-dependent fluorophore effects. Data
1004 represent the mean ± s.d. (n=3). **e**, TR-FRET titration of CDK13-$_{Alexa488}$cycK (0-3.75 µM) to 50 nM
1005 $_{Terbium}$DDB1 and 5 µM CR8 or DMSO. Data represent the mean ± s.d. (n=3). **f**, TR-FRET titration of
1006 CDK9-$_{Alexa488}$cycK (0-3.75 µM) to 50 nM $_{Terbium}$DDB1 and 5 µM CR8 or DMSO. Data represent the
1007 mean ± s.d. (n=3). **g**, *In vitro* ubiquitination of cycK by the RBX1$_{N8}$CUL4-DDB1 ubiquitin ligase core
1008 in the presence of CDK12, CDK13 or CDK9. **h**, TR-FRET titration of CDK12-$_{Alexa488}$cycK (CDK12
1009 mutant (L1033A, W1036A); 0-3.75 µM) to 50 nM $_{Terbium}$DDB1 and 5 µM CR8 or DMSO. Data
1010 represent the mean ± s.d. (n=3). **i**, TR-FRET titration of CDK12-$_{Alexa488}$cycK (CDK12 tail truncation
1011 (713-1032); 0-3.75 µM) to 50 nM $_{Terbium}$DDB1 and 5 µM CR8 or DMSO. Data represent the mean ±
1012 s.d. (n=3).
1013
1014
1015
1016
1017
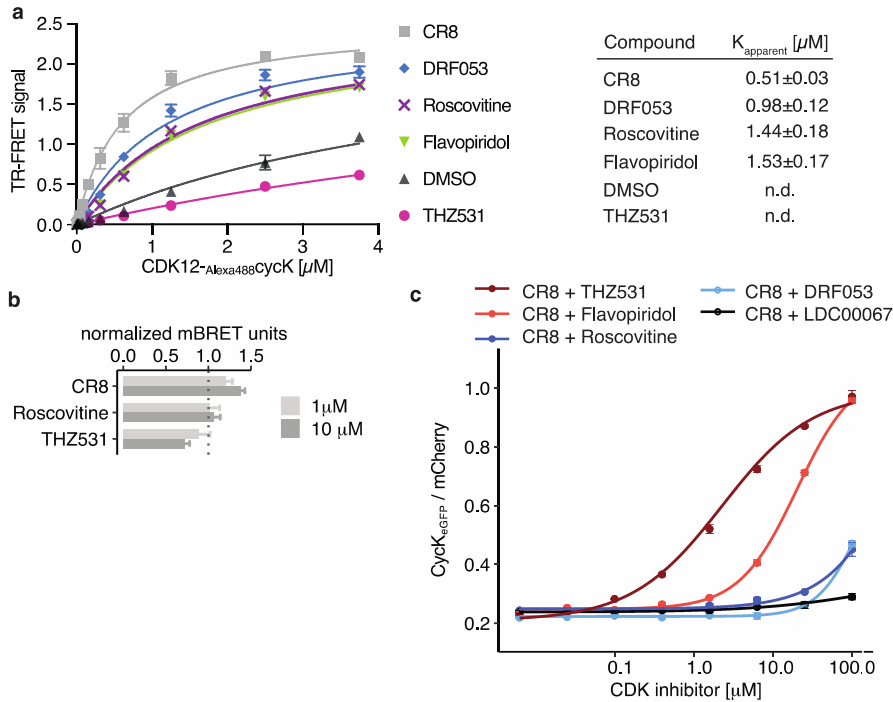
Extended Data Figure 8 | CDK inhibitors block CR8-induced cycK degradation. a, TR-FRET. CDK12-$_{Alexa488}$cycK titrated to $_{Terbium}$DDB1 in the absence (DMSO) or presence of 10 μM CR8, roscovitine, DRF053, flavopiridol or THZ531. Data represent the mean ± s.d. (n=3). **b**, HEK293T cells transiently transfected with $_{NanoLuc}$CDK12$^{713-1052}$ and $_{HaloTag}$DDB1^{ΔBPB} constructs were treated with DMSO or inhibitors for 2 hours and the mBRET signal was measured. Data represent the mean ± s.d. (n=3). **c**, CycK$_{eGFP}$ HEK293T$_{Cas9}$ cells were treated with 1 μM CR8 and varying concentrations of competitive CDK inhibitor and analysed by flow cytometry. Data represent the mean ± s.d. (n=3).
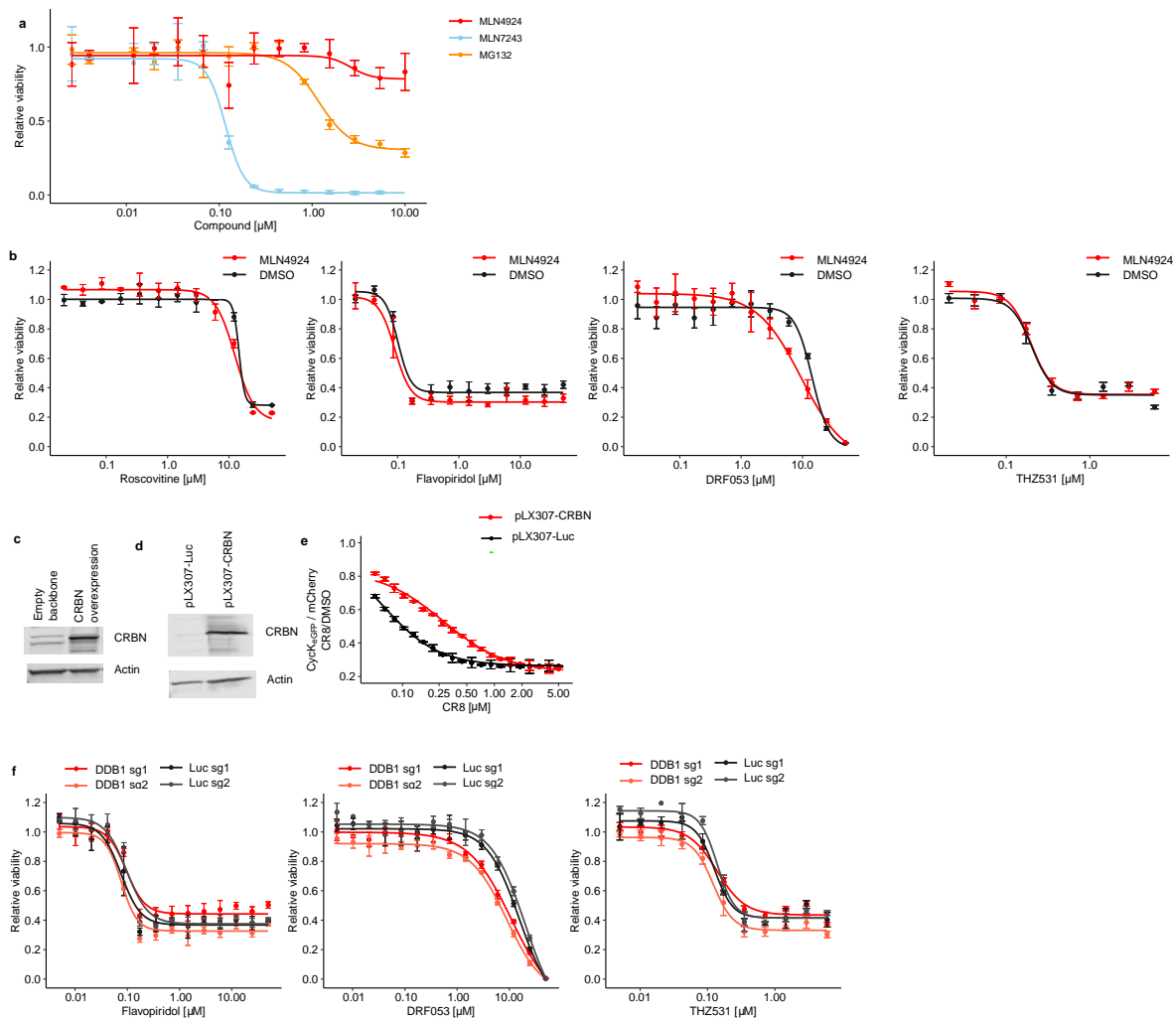
Extended Data Figure 9 | Cytotoxicity of CR8 analogues does not depend on CRL4 components. **a**, HEK293T$_{Cas9}$ cells were exposed to indicated concentrations of MLN4924, MLN7243 or MG132 for 3 days. Data represent mean ± s.d. Lines represent standard four-parameter log-logistic curves. **b**, HEK293T$_{Cas9}$ cells were exposed to DMSO or 100 nM MLN4924 in combination with indicated concentrations of roscovitine, flavopiridol, DRF053 or THZ531 for 3 days. Data represent mean ± s.d. Lines represent standard four-parameter log-logistic curves. **c, d**, HEK293T$_{Cas9}$ cells were transiently transfected with control or CRBN overexpression vector and after 48h lysates were immunoblotted for the indicated targets. pRSF91-GFP and pRSF91-CRBN are denoted as empty backbone or CRBN overexpression respectively. **e**, CycK$_{eGFP}$ HEK293T$_{Cas9}$ cells were transiently transfected with control or CRBN overexpression vector and after 48h were exposed to the indicated concentrations of CR8 for 2h and analysed by flow cytometry. Data represent mean ± s.d. Lines represent standard four-parameter log-logistic curves. **f**, HEK293T$_{Cas9}$ cells were transduced with sgRNAs targeting DDB1 or luciferase and exposed to the indicated concentrations of CR8, roscovitine or DMSO for 3 days. Data represent mean ± s.d. Lines represent standard four-parameter log-logistic curves.

Extended Data Table 1 | Data collection and refinement statistics.

	DDB1$^{\Delta BPB}$-CR8-CDK12$^{713\text{-}1052}$-CycK$^{1\text{-}267}$
Data collection	
Space group	$P3_121$
Cell dimensions	
a, b, c (Å)	250.75, 250.75, 217.92
α, β, γ (°)	90, 90, 120
Resolution (Å)	54–3.46 (3.63–3.46)*
R_{meas}	0.318 (>4.00)
$I/\sigma I$	7.2 (0.9)
Completeness (%)	95.1 (68.3)[†]
Redundancy	12.0 (11.6)
Refinement	
Resolution (Å)	54–3.46
No. reflections	89,183
R_{work} / R_{free}	0.1934 / 0.220
No. non-hydrogen atoms	
Protein	33,781
R-CR8	96
B-factors (Å^2)	
Protein	59.9
R-CR8	39.6
R.m.s. deviations	
Bond lengths (Å)	0.009
Bond angles (°)	1.01

*Values in parentheses are for the highest-resolution shell.

[†] From STARANISO (REF) assuming a local weighted $CC_{1/2} = 0.3$ resolution cut-off

1051 **Supplementary Information Guide**

1052 **Supplementary Tables:**
1053 Supplementary Table 1. Oligonucleotides used in this study
1054

1055 **Supplementary Data:**

1056 **Data for 158 E3 gene-compound pairs identified in bioinformatic screen**

1057 **Primary data for validation of 96 E3 gene-compound pairs**

1058 **Proteome quantification using tandem mass tag spectrometry data**

1059 **Functional genomics data**

1060 **Supplementary isothermal titration calorimetry (ITC) data**

1061 **Uncropped Western blots and SDS-PAGE gels**

1062 **wwPDB X-ray structure validation report**

1063

1064 **Supplementary Code:**

1065 **Code used for bioinformatic screen to identify E3-drug ligase pairs**

1066 **Code used for validation of 96 E3 gene-compound pairs**

1067 **Code used for identification of hits in genome wide CR8 resistance screen for single**

1068 **replicate**

1069 **Code used for identification of hits in CR8 resistance and cyclin K stability screens for**

1070 **multiple replicates**

1071